AMERICAN UNIVERSITY OF BEIRUT

AN IMPROVED MODEL OF FOREBRAIN-PROJECTING CORTICAL NEURONS IN THE OSCINE SONGBIRDS

by
MIRA FAYAD

A thesis
submitted in partial fulfillment of the requirements
for the degree of Master of Science
to the Biomedical Engineering Program
of the Maroun Semaan Faculty Engineering and Architecture and Faculty of Medicine
at the American University of Beirut

Beirut, Lebanon
May 2018

AMERICAN UNIVERSITY OF BEIRUT

AN IMPROVED MODEL OF FOREBRAIN-PROJECTING CORTICAL NEURONS IN THE OSCINE SONGBIRDS

by

MIRA FAYAD

Approved by:

[Dr. Arij Daou, Assistant Professor] Advisor
[Biomedical Engineering Program]
Maroun Semaan Faculty of Engineering and Architecture

[Dr. Firas Kobeissy, Associate Professor] Co-advisor
[Department of Biochemistry and Molecular Genetics]
Faculty of Medicine

[Dr. Zaher Dawy, Professor] Member of Committee
[Department of Electrical and Computer Engineering]
Maroun Semaan Faculty of Engineering and Architecture

[Dr. Fadi Karameh, Associate Professor] Member of Committee
[Department of Electrical and Computer Engineering]
Maroun Semaan Faculty of Engineering and Architecture

Date of thesis defense: [May 02, 2018]

AMERICAN UNIVERSITY OF BEIRUT

THESIS, DISSERTATION, PROJECT RELEASE FORM

Student Name:

Fayad	Mira	
Last	First	Middle

● Master's Thesis ○ Master's Project ○ Doctoral Dissertation

[X] I authorize the American University of Beirut to: (a) reproduce hard or electronic copies of my thesis, dissertation, or project; (b) include such copies in the archives and digital repositories of the University; and (c) make freely available such copies to third parties for research or educational purposes.

I authorize the American University of Beirut, to: (a) reproduce hard or electronic copies of it; (b) include such copies in the archives and digital repositories of the University; and (c) make freely available such copies to third parties for research or educational purposes

after : **One ---- year from the date of submission of my thesis, dissertation, or project.**

Two ---- years from the date of submission of my thesis, dissertation, or project.

Three ---- years from the date of submission of my thesis, dissertation, or project.

May 14, 2018

Signature Date

This form is signed when submitting the thesis, dissertation, or project to the University Libraries

ACKNOWLEDGMENTS

First, I would like to thank my thesis advisor Dr. Arij Daou for his continuous support throughout the last two years, and for introducing me to the songbird field.

I would also like to thank the rest of my thesis committee: Dr. Zaher Dawy, Dr. Fadi Karameh, and Dr. Firas Kobeissy for their encouragement and insightful comments.

My sincere thanks goes to Dr. Daniel Margoliash of the Department of Neuroscience at the University of Chicago, for inviting me to collect my data at his lab.

Finally, I am profoundly grateful to my parents whose love and guidance are with me in whatever I pursue. I am also thankful to my brother and my best friend Yasmine for providing me with unwavering support and endless reassurance throughout the process of researching and writing this thesis. This accomplishment would not have been possible without them. Thank you.

.

AN ABSTRACT OF THE THESIS OF

Mira Fayad for Master of Science
Major: Biomedical Engineering

Title: An Improved Model Of Forebrain-Projecting Cortical Neurons In The Oscine Songbirds

Since the late 1960s, songbirds have emerged as a notable neurobiological model for studying aspects of human verbal communication. Songbirds learn to arrange their song elements, analogous to how humans learn to produce spoken sequences with syntactic structure. One of the most fundamental questions in neuroscience is pursued through the study of songbirds, more specifically through the study of zebra finches. Questions on how the brain generates complex sequential behaviors and the neural mechanisms that underlie sequential behavior are the holy grail of the neuroscience field.

The telencephalic nucleus HVC (proper name) within the songbird, analogue to the mammalian pre-motor cortex, is situated at a critical point in the pattern-generating premotor brain circuitry of oscine songbirds. HVC contains three interconnected populations of neurons, HVCRA (projecting to forebrain), HVCX (projecting to basal ganglia) and HVCINT (interneurons), which possess specific patterns of excitatory and inhibitory connectivity. HVCRA neurons were of particular interest in this research due to their significance in the propagation of sequential activity, which encodes the zebra finch's song. Whole-cell intracellular recordings were collected from HVCRA neurons within zebra finch brain slices. The biological data collected was used to create and calibrate a conductance-based HVCRA model. The mathematical model unveiled the expression of important ionic currents, which govern the dynamics of these neurons and that are presumably playing an imperative role in the rhythmogenesis that this cortical area exhibits during singing. The new model allows for a better understanding of the ionic currents responsible for HVCRA's characteristic sparse bursting firing patterns. The presence of the ionic currents could later be tested and verified using neuropharamacology.

CONTENTS

ILLUSTRATIONS

TABLES

CHAPTER 1
LITERATURE REVIEW

1.1 Behavioral Resemblance in Birdsongs and Human Speech

In 1872, Charles Darwin recognized the similarities between human speech in infants and song learning in songbirds [1]. Earlier studies of human speech were strictly behavioral. Upon Darwin's discovery, birdsong researchers and bio-linguistics were encouraged to document the cognitive, neural and molecular parallels in the two species [2]. Recognition of the similarities between birdsong and human speech militated neurological and ultimately electrophysiological breakthroughs in the structure and connectivity of the vocalization-related brain regions in humans, through songbird research [2].

1.1.1 The Song Learning Process

Parallels between humans and songbirds are most apparent in the fact that the two species learn their "language" in early life stages, both imitating an adult of the same species and consolidating this language throughout adulthood [2]. Songbirds also acquire only one song and sing it throughout their lifetime, similar to how humans have a first or native language [3]. The "one song" property in songbirds excited researchers, as it provided a control to be compared to when studying the effects of varying learning parameters in humans [3]. These resemblances led to further comparisons between the two species in terms of the learning stages of vocalization [2].

In 1967, Lenneberg strongly claimed that prior to puberty, language learning in humans is at its critical period [4]. Post puberty, learning abilities deteriorate due to hormones, making newly acquired languages more labored and consciously articulated, which results in what is known as an "accent" [4]. Likewise, songbirds learn the tutor's song best in their early life, and once learned, the song remains strikingly stereotyped [3]. This similarity particularly allowed for studies of the neural mechanisms of brain plasticity in adult life for human learning by studying songbird's brain regions; both electrophysiologically and at the molecular level [2, 3].

Aside from the existence of a critical period for language learning in both species, the stages of learning in songbirds and humans are also very similar [2, 3]. The first or the sensory stage of song learning involves listening and memorization of the tutor song in songbirds, and is similar to the early perceptual learning stage in human infants [2, 3]. Humans and songbirds are assumed to have natural perceptual inclination for the vocal behavior of their own species, but what is acquired in this stage is significant since it is later used to guide vocal production or vocalization [2, 3].

The second stage of vocal learning in both species is undeveloped vocalizations or in other words the sensorimotor stage, where human infants "babble", and young songbirds produce what is known as "subsongs" [2, 3]. In later stages, these sounds are developed into crystallized adult vocalizations. However, as mentioned earlier, the first phase is critical, so experience influences vocalization in both species. When in isolation, songbirds sing abnormally in a form called the "isolate song" [2], though when young birds are taught

an isolate song, they improve their song to a more species specific form. This resonates what is seen in human children that are more grammatically correct than their parents [2, 3]. Isolation effects on humans are understood through studies performed on children raised in remote settings, where they developed abnormal vocalizations similar to the isolate song in songbirds [2, 3]. This shows that learning is not only based on innate predispositions, but also on social factors in both species.

Once both species learn and vocalize their language, auditory feedback plays a major role in the third stage or the plastic stage for both songbirds and humans [2]. Auditory feedback in the case of songbirds is the comparison of the vocalized song with the template or stored tutor song, as well as the adjustment of the song accordingly to match the tutor song [2]. The relevance of auditory feedback in both species is evident since congenital deafness showed differences in babbling for humans and in "sub-songs" for songbirds at the second stage of vocalization [3]. Deafness in human adults deteriorates speech less effectively than in infants, since adults have their speech formed, whereas at the first stage of learning, infants are learning to vocalize from what they hear. Adult songbirds however, showed little deterioration in their song after induced deafness, suggesting that songbirds have a non-auditory feedback pathway or a central pattern generator [3]. Nevertheless, both species (young and adult) show vocal deterioration when delayed auditory feedback is played, indicating similarities in the auditory pathways between the two species, and signifying that auditory feedback plays a role in maintaining vocalization throughout their lifetime [3].

The final stage of vocal learning in songbirds is when the song is in its crystallized form; in other words, the tutor song is properly vocalized. In terms of human language, humans can speak properly at this stage [3]. However, learning is a continuous process in both species with auditory feedback maintaining proper vocalization throughout their lifetime [3].

In terms of language interpretation, songbirds and humans are very different, but the staggering similarities in vocal learning encouraged research in the neural mechanisms of vocal production pathways in songbirds to explain the behavioral similarities [3]. One of the most common songbirds used as an avian model to study the neural bases of learning is the zebra finch [5]. It's popularity in research is due to its prolific breeding and adaptation to the dry environment common in labs [5]. More importantly, once the zebra finches learn their song, they repeat the same notes with extreme precision with no changes, unlike canaries or other species of songbirds that keep updating the structure of their notes through their adulthood [5].

The male zebra finches learn and sing a template song, and they do so to attract a female mate [5]. The female zebra finches however do not sing a template song [5]. This gender specificity has been related to that fact that male zebra finches have an elaborate neural system comprised of several nuclei that are known collectively as the "song system", while female zebra finches do not exhibit this system.[5].

1.1.2 Basic Units of Song

To further study songbirds as a model for speech learning, researchers broke down birdsongs into 3 basic units of song: the syllable, the motif, and the bout [6]. The song syllable is the basic acoustic element in a birdsong; it is made up of a complex sequence of sounds changing over 200ms or less, and is considered as the largest unit of vocalization [6, 7]. The song motif is considered as several different song syllables organized in one pattern and repeated over a 1s timeframe, separated by gaps. The song bout is described as 2 to 3 second bursts of song elements rapidly composed in succession during a subsong [8]. A spectrogram depicts the pschyschoachoustics of birdsongs (Figure 1) where song bouts are shown in the different stages of song learning in songbirds as described above.

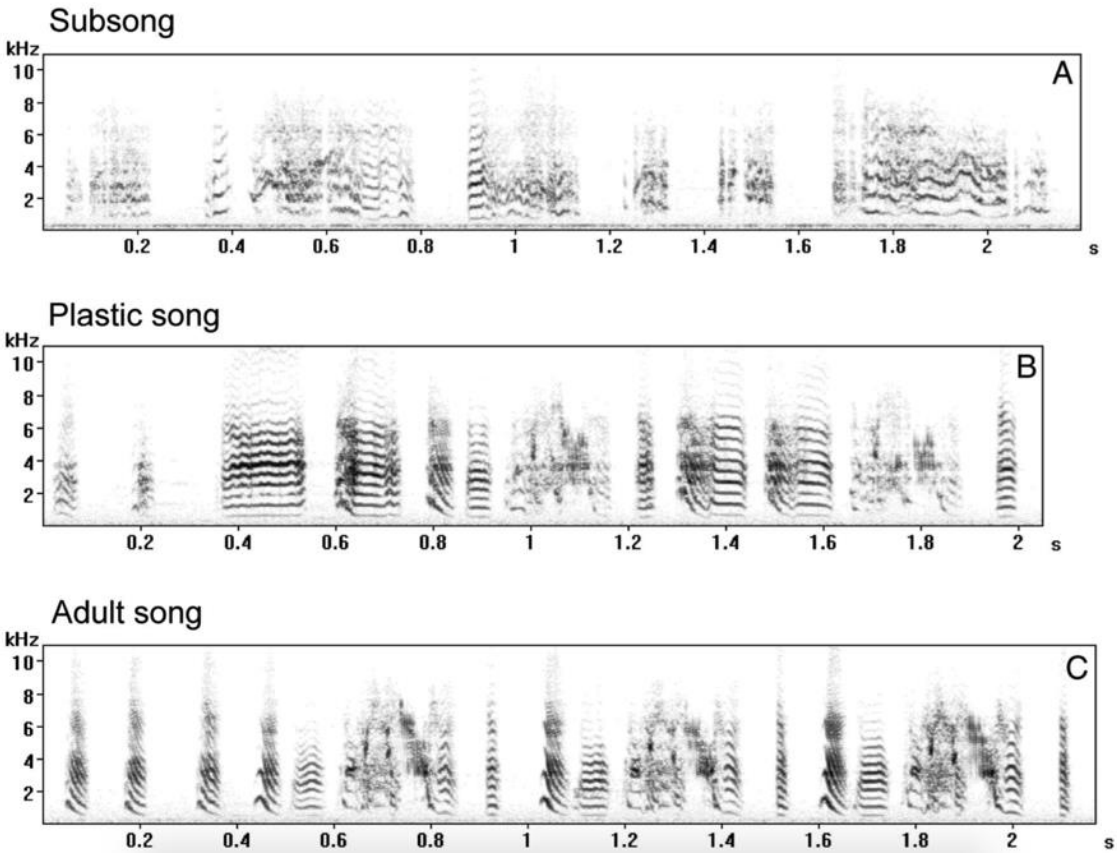

Figure 1: Spectrogram showing the three stages of song learning in songbirds, when the same bird is singing a subsong, plastic song and adult song [8]. Through continuous rehearsal, the temporal and spectral features of the song become "crystallized", leading to a temporally precise and reproducible song (adult song) that the zebra finch keeps singing for the rest of his life.

1.1.3 The Song System Anatomy

The male zebra finch has been studied thoroughly and scientists have agreed on a model for the acquisition and production of birdsongs through a set of forebrain nuclei that form a well-characterized network called the "Song System" (Figure 2) [9, 10].

During song learning and production, the two most relevant pathways in the song system are the AFP (anterior forebrain pathway, the red pathway in Figure 2) and the VMP

(vocal motor pathway, the blue pathway in Figure 2) [10]. Both pathways originate at nucleus HVC (proper name) of the dorsal pallium. The AFP is a recursive loop pathway important in song development, and indirectly connects HVC to RA (Robust Nucleus of the Arcopallium) [10]. The VMP is a pathway important in vocal production since it directly connects HVC to RA and RA in turn projects to the nXIIts (tracheosyringeal nucleus of the XII cranial nerve), which in turn regulates the muscles of the syrinx [10]. Both pathways are represented in Figure 2, where area X is the nucleus of the basal ganglia, DLM is the medial nucleus of the dorsolateral thalamus in the diencephalon, and LMAN is the lateral magnocellular nucleus of the anterior nidopallium [10].

In the AFP, area X is the basal ganglia nucleus responsible for song learning, recognition of the bird's own song, and it is also responsible for the song tempo and global syllable sequencing and so prevents syllable repetition or stuttering [11]. Area X also controls pitch variability in adult birds [12]. DLM indirectly links HVC to RA, and when inhibited by inhibitory synapses in area X, it creates excitatory synapses on neurons in LMAN [13]. Axons from LMAN send variable bursting activity that drives song variability and adjustment through the excitatory connections it makes with RA neurons, making it the major basis of auditory input to RA and giving it a role in song maintenance and error correction that influences the motor pathway in terms of auditory feedback, and so encodes a lasting template of a tutor song [13]. RA auditory neurons have song selectivity similar to LMAN [12]; a collection of RA auditory neurons drive variable performance, which is an important feature in song learning as it indicates customizability of birdsongs [13].

In the VMP, RA motor neurons provide a song output from the HVC to the syrinx, as electrophysiological recordings of RA show that RA neurons burst at the same time the bird is singing [14]. NXIIts is the syrinx or the songbird's vocal organ responsible for song output controlling the musculature that generates the vocal sounds [15]. DM is located in the midbrain; it receives projections from RA, this explains its role in song production, and it also innervates nXIIts, which explains its role in respiratory vocal control [15]. Other pathways are also depicted in Figure 2, where the green pathway is presumed to be important in outlining the arrangement of units sung in a song. The purple pathway is alleged to have a function in establishing the respiratory activity required for song production. The orange pathway connects AFP to the VMP through HVC. The grey pathway represents the auditory pathways, and responses in this pathway's nuclei are customized to the bird's own song. Finally the yellow pathway contains nuclei that send dopaminergic inputs to area X [10]. These pathways are equivalent in humans and songbirds since they share a complex hierarchy that is similar in many ways as shown in Table 1.

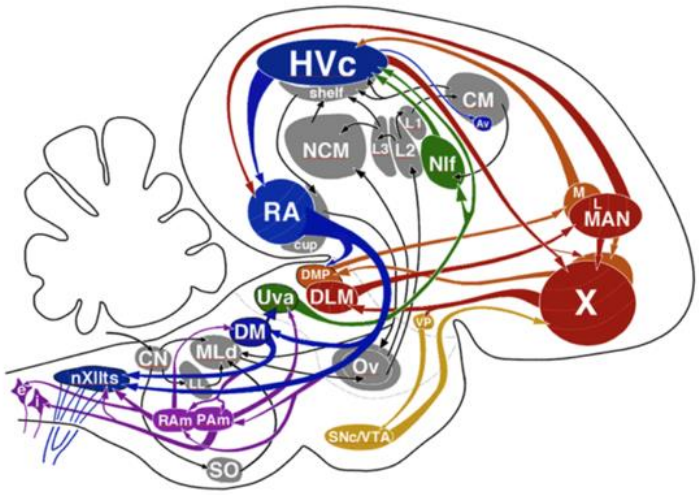

Figure 2: A sagittal section of the "song system". The blue pathway is the vocal motor pathway (VMP), red is the anterior forebrain pathway (AFP), orange connects VMP and AFP through HVC, grey is the auditory pathway, the yellow pathway sends dopaminergic input to area X, the purple pathway controls the respiratory musculature, and the green pathway is relevant in song arrangement [10].

Table 1: Human and songbird neural components of vocal production in the forebrain [2, 9, 10].

Function	Human brain region	Songbird brain region
1- Language development, comprehension of speech 2- Production of speech	1- Wernicke's area 2- Broca's area	HVC
1- Involved in learning 2- Vocal motor control and speech production	1- Cingulate cortex 2- Motor cortex	RA (robust nucleus of the arcopallium)
1- Control of voluntary movement/ speech 2- Relays motor and sensory signals	1- Basal Ganglia 2- Thalamus	1- area X/LMAN 2- DLM

1.2 Nucleus HVC: The Cortical Maestro of Vocalization

HVC is a paramount auditory vocal interface due to its prominence in the AFP and VMP pathways [16]. HVC is essentially important in both song production and learning. During the sensorimotor stage in songbirds, birds tend to prefer their own song or what is known as BOS (bird's own song). HVC neurons have been found to have a preference to the BOS suggesting that HVC plays an important role in song production in the plastic song phase [2]. Also, at the level of HVC, encoding of the temporal sequence of song elements occurs where a single neuron explicitly codes for a syllable [7]. HVC has multiple inputs and outputs from and to the song system's nuclei, which is why HVC acts as an essential site of information assimilation and distribution [7]. All auditory neurons in HVC possess selective response to the BOS, with time and acoustic sensitivity, making HVC the integrator of auditory response [7]. This has strong implications on the role that HVC plays in memory consolidation of the song, since HVC neurons tend to fire in the same way while the bird is sleeping just like when he is singing [7]. Moreover, HVC neurons show similar single neuron auditory properties between the same bird and a development of these properties among the same neurons, linking HVC to song development [7].

The connection between HVC and the nuclei in the song system is carried through projecting neurons. The projecting neurons leaving HVC are HVC_{RA} (to RA) and HVC_{X} (to area X). HVC also contains interneurons (HVC_{INT}) that stay within HVC and innervate both classes of projection neurons [17].

HVC_{RA} neurons show inhibited firing patterns when the bird sings, and only fire in brief bursts during a motif at a precise time sequentially [6, 14]. The collection of HVC_{RA} neurons burst at the same time, eliminating the temporal effect during sequential activation of HVC_{RA} neurons. This shows that HVC_{RA} neurons are activated sequentially in chain-like manner, where neural impulses are propagated synchronously between nuclei [6], reiterating the importance of HVC in song timing, since the timing of a song set in HVC is not lost during impulse propagation between nuclei [14].

HVC_{RA} and HVC_X possess an inhibitory and excitatory synaptic linkage, this synaptic linkage helps shape the pattern of HVC_X while the bird is singing to allow the bird to refine its song [18]. HVC_X also innervates the AFP, which shows how HVC's local circuitry shapes and conveys premotor activity to the AFP [18]. HVC_{INT} innervates HVC_{RA} and HVC_X, synchronizing the firing of multiple HVC neurons, and as a result synchronizing HVC's activity [18]. In particular, interneurons are known to inhibit both classes of projecting neurons (HVC_X and HVC_{RA}) via GABAergic pathways, and in return both classes of projecting neurons are known to send excitatory signals to interneurons via NMDA and AMPA pathways [18]. There is no known monosynaptic connection from HVC_{RA} to HVC_X, these two classes interact with one another disynaptically via HVC_{INT} as the intermediary with HVC_{RA} having an inhibitory effect on HVC_X.

The three projecting neurons extend within HVC, allowing for local synaptic processing. This partakes the importance of HVC in premotor activity, specifically in song refinement during song learning due to local excitement and inhibition of HVC_{RA} neurons

[18]. In song motor activity, HVC's relevance is echoed due to HVC_{RA} and HVC_X coupling within HVC [18]. $HVC_{X,}$ HVC_{INT}, and HVC_{RA} possess different functions and can be distinguished morphologically and electrophysiologically [19].

1.2.1 Morphological Identification of HVC

HVC is heavily myelinated, which makes it easy to identify as a dark region in a brain slice when transilluminated and observed through a light microscope (Figure 3A). Once HVC is identified, its projecting neurons; $HVC_{X,}$ HVC_{INT}, and HVC_{RA} can be identified through retrograde labeling of area X and RA, which then allows the projecting neurons to be identified by epifluorescence illumination [19]. Focal infusion of rhodamine or DiI and DiO into area X and RA respectively *in vivo* is the approach to retrogradely label HVC_X and HVC_{RA} neurons (Figure 3B) [19]. Conjunction of both trans and epifluorescence illuminations allows for projecting neuron identification in HVC (Figure 3C) [19]. Neurons that are not fluorescently labeled are assumed to be HVC_{INT} neurons [19]. When anatomical identification is required, projection neurons can be differentiated by the size of their soma, the length of their projecting axons and their dendritic extent (Figure 4). Moreover, HVC neurons exhibit distinctive anatomical features that make their identification further confirmed once they are filled intracellularly with biocytin or neurobiotin (Figure 5).

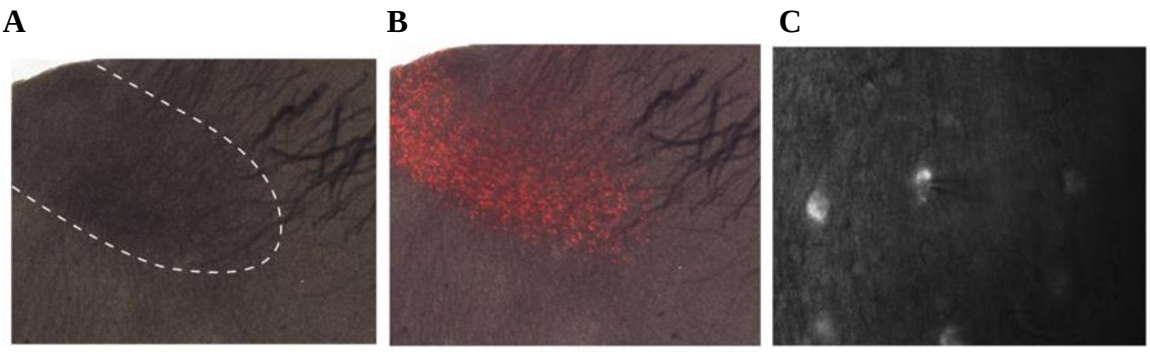

Figure 3: Morphological identification of HVC projecting neurons where **A** represents locating HVC, **B** represents localizing HVC_X through retrograde labeling and **C** shows how patching into an identified projecting neuron from the conjunction of transillumination and epifluorescent illumination is made possible. Image adopted from Daou et al. [19].

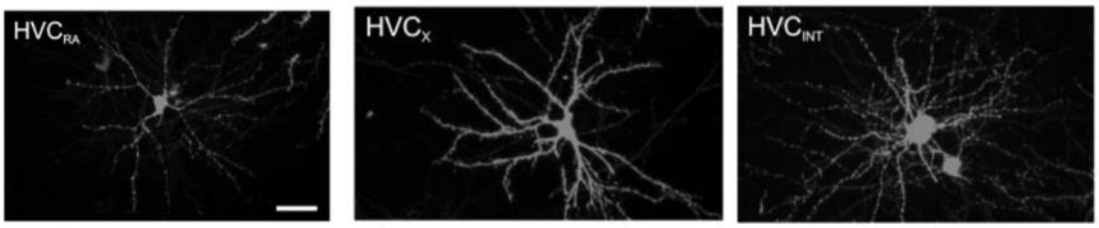

Figure 4: Anatomical identification of HVC projecting neurons [18]. HVC_{RA} neurons exhibit a small soma compared to HVC_X, which is even smaller when comparing it with the soma of HVC_{INT} neurons. Also, interneurons of HVC as well as X-projecting neurons exhibit a large number of spines compared to RA-projecting neurons.

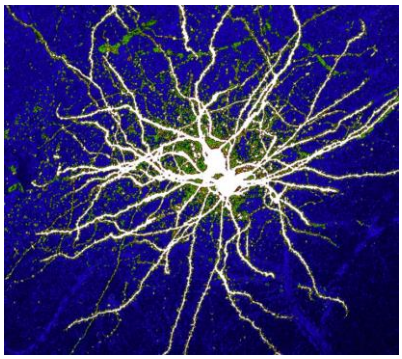

Figure 5: HVC_{RA} and HVC_{INT} neurons filled with biocytin for clearer anatomical identification. Neurotransmitters can be seen surrounding soma of HVC. Image adopted from Daou and Margoliash, under review.

1.2.2 Electrophysiological Identification of HVC Neurons

Electrophysiology is the study of the electrical activity in physiological models. The electrophysiology of a songbird's HVC neurons can be classified according to their electrophysiological properties as studied in earlier literature [16, 17, 20, 21]. Recent studies have shown more detailed differences in the electrophysiological identifications of HVC projecting neurons [19]. The three classes of HVC neurons exhibit very distinctive firing patterns orchestrated by the intrinsic expression of a mixture of ionic channels. For instance, in terms of response to depolarizing current pulses, HVC_{INT} neurons fire action potentials with high frequency exhibiting little to no adaptation (Figure 6A), while HVC_X neurons fire a train of spikes with less frequency (Figure 6C) and exhibits moderate spike frequency adaptation (SFA, the feature characterized by the interspike intervals starting small in duration and then increasing in duration over the course of current application) [19]. On the other hand, HVC_{RA} neurons fire with one or few action potentials and show very strong adaptation (Figure 6E). In regards to voltage response to hyperpolarizing current pulses, HVC_{INT} neurons present a very prominent sag accompanied by strong rebound firing at the end of the negative current pulse (Figure 6B), HVC_X neurons reveal little sag with moderate rebound firing (Figure 6D), while HVC_{RA} neurons present no sag at all. [19]. Concerning the resting membrane potential (RMP), HVC_{RA} neurons demonstrate a potential of around -85 mV RMP, HVC_X neurons around -72 mV RMP and HVC_{INT} around -60 mV [19].

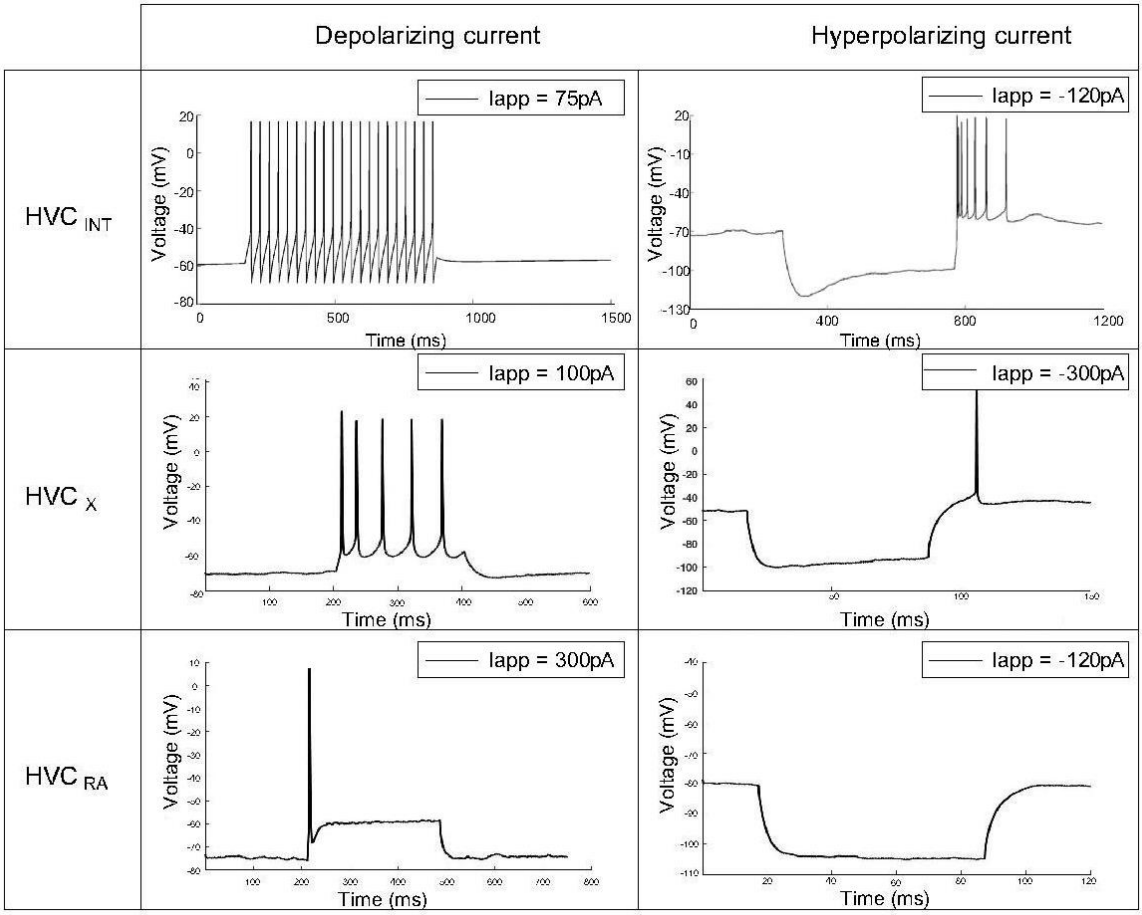

Figure 6: Electrophysiological identification of HVC projecting neurons in response to depolarizing and hyperpolarizing current pulses. When stimulated with a positive pulse, interneurons exhibit high frequency firing with no adaptation, while HVC_X fires tonically with adaptation and HVC_{RA} fires one or two spikes with very strong adaptation. In response to negative pulses, interneurons exhibit very prominent sag followed by rebound, while HVC_X exhibit a less prominent sag and HVC_{RA} shows no sag.

1.2.3 Latest Model of HVC

In 1952, Hodgkin and Huxley (H-H) conducted a series of experiments to study the laws of ionic movements in nerve cells when neurons burst action potentials [22]. The sum of all those experiments were created into what is known as the H-H model, and its laws were later referenced in neuroscience research to recreate properties of HVC projecting neurons firing patterns [19].

In 2013, Daou et al. completed the latest model describing HVC neuronal dynamics [19]. Each of the ionic currents integrated in the model was tested and verified in the slice using neuropharmacology. In particular, HVC neuron's membrane potential followed the following equation:

$$C_M\frac{dV}{dt} = -I_L - I_K - I_{Na} - I_{Ca-T} - I_{Ca-L} - I_A - I_{SK} - I_{KNa} - I_h - I_{Nap} + I_{app}$$

Where I_{app} represents the constant applied current, C_M is the membrane capacitance, spike producing currents are I_K and I_{Na}, a leak current I_L, a low-threshold T-type Ca^{2+}current $I_{Ca\text{-}T}$, a high-threshold L-type Ca^{2+}- current $I_{Ca\text{-}L}$, a small-conductance Ca^{2+}-activated K^+ current I_{SK}, a hyperpolarization-activated cation current I_h, a Na^+ -dependent K^+ current I_{KNa}, a persistent Na^+ current I_{Nap}, and an A-type K^+ current I_A [19, 23].

I_K indicates the presence of standard potassium current, I_{Na} indicates the presence of standard sodium current, I_L indicates leak in the cell membrane. $I_{Ca\text{-}L}$ indicates burst firing, $I_{Ca\text{-}T}$ indicates post-inhibitory rebound firing, I_{SK} and I_{KNa} independently indicate the presence of adaptation, and I_h indicates the presence of sag after hyperpolarizing an HVC projecting neuron. I_{Nap} indicates a plateau potential in response of depolarizing current, and

I_A indicates the presence of delay in an action potential in response to depolarizing pulse [19, 23]. This model is visually described (Figure 7) as an electrical circuit.

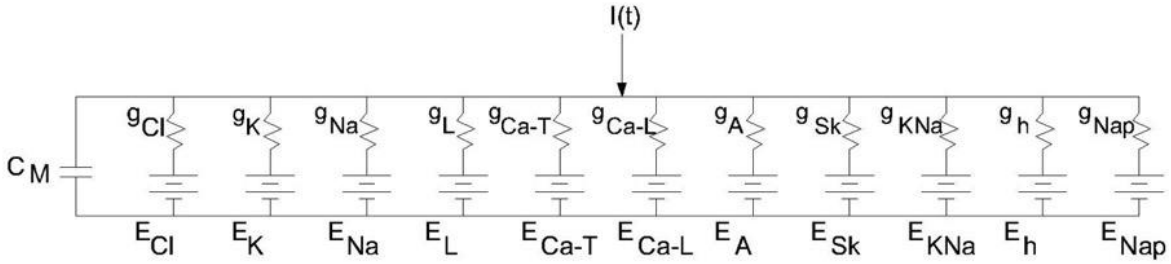

Figure 7: General H-H model for HVC projecting neurons.

CHAPTER 2

INTRODUCTION

Several neurodegenerative diseases have been recently found to be due to a one-ionic channel mutation characteristic [24]. Ionic channels are imperative in neural mechanisms due to their signal control role of allowing ions in or out of a neuron. Disturbances of neural ionic channels by their overexpression or repression [25] is a major cause of diseases, categorized as neural channelopathies [24]. The study of ionic channels allows for a better understanding of channelopathies, and as such instigates for a treatment of ionic imbalances by drug-blocking of overexpressed channels or drug-activation of repressed channels [24].

To better understand the ionic imbalances in neurodegenerative diseases, electrophysiological studies have been carried out over the past decade to discover a link between neurodegenerative diseases in the central nervous system (CNS) associated with mutations in ionic channels [26]. Consequently, many CNS disorders including epileptic syndromes were identified as neural channelopathies [26]. For instance, generalized epilepsy with febrile seizures is triggered by mutations in the voltage gated potassium channels [26]. Similar discoveries allowed for the development of drugs for neurodegenerative disorders such as Alzheimer's disease (AD) where a drug that counteracts the depletion of potassium channels is administered to maintain normal dendritic excitability and synaptic plasticity of neurons. Blocking calcium entry into

neurons now treats late onset AD. Also, Parkinson's disease cell loss can now be controlled using an antagonist for Ca^{2+}-L channels [25].

Neurodegenerative diseases such as dementia and AD have been found to cause vocal deterioration [24]. To understand the ionic channel imbalances causing vocal deterioration in the hopes of reversing it, songbirds, specifically zebra finches, have been used as a model. HVC is the cortical maestro of vocalization in zebra finches, and so understanding the network of HVC would allow for the identification of the ionic channel cocktail governing vocalization neurons. Modeling HVC is the way to accomplish that.

The existing model of HVC projecting neurons in zebra finches developed by Daou et al. in 2013 can replicate the firing patterns of HVC_X and HVC_{INT} neurons accurately, but fails to do so for HVC_{RA}. In order to connect HVC neurons in circuits and better understand the functionality of this nucleus, an improved model for HVC_{RA} is needed [19]. The current HVC_{RA} model shows discrepancies with experimental data, one of which is the difference in neuron activity with 100pA current application [19], where the model shows no activity and the actual neurons fires with low frequency [19]. In the paper published in 2013, it was also difficult to study the effect of blocking potassium dependent sodium current I_{KNa} due to the ambiguity of the current blockage from using quinidine as a nonselective blocker of I_{KNa} in the experiment. The ambiguity of the current blockage made it challenging to deduce what mixture of blocked currents produced the observed firing pattern, and so, prohibited the study of bursting patterns in HVC_{RA} *in vivo* [19]. Moreover, contrasting the model, the HVC_{RA} neurons exhibit no adaptation in response to blocking calcium

dependent potassium current I_{SK}, when they should according to experimentation [19]. The model-experiment differences encouraged further research for understanding the physiological characteristics of HVC_{RA}.

An improved model will allow for a better understanding of the firing patterns and characteristics of ionic currents present in HVC_{RA}. Once HVC_{RA}, HVC_X and HVC_{INT} firing patterns are fully understood, the neuroscience society would have a control model for firing patterns in the neurons of this cortical area. This is of significance to the songbird community for two significant reasons, one of which is a better understanding of the reason behind the dramatic effects on the spectral and temporal features of song, where sequential propagation of activity is disrupted after changes in the firing pattern of HVC_{RA} neurons *in vivo* (Daou & Margoliash, under review).

Once a control model is developed for HVC, experiments could be performed on songbirds to induce the ionic channel mutation effects on vocalization. HVC projecting neuron's electrophysiology would then be collected and compared with the control model. Such comparison would allow for the understanding of which ionic channels were blocked or activated, affecting vocal gestures [27]. Hence, as a treatment method at the level of human vocalization, blocking or inducing a certain ionic channel could reverse the effect on vocalization deterioration in neurodegenerative diseases.

This thesis presents an improved model of HVC_{RA} to allow for a better understanding of the ionic channels involved in HVC. The model was completed through electrophysiological data collection, model fitting and model testing. Model tests proved

the model accurate in replicating the firing patterns of HVC_{RA} due chaotic stimuli, giving significant implications on the constituents of ionic currents that are responsible for the rhythmogenesis seen *in vivo* during singing.

CHAPTER 3

METHODOLOGY

3.1 Data Collection

As mentioned in Chapter 1, adult male zebra finches are the most ideal songbird model to study human speech and vocalization. Data was collected from zebra finches in a neuroscience lab at the University of Chicago in Dr. Daniel Margoliash's lab upon his support and approval. Twelve zebra finches were utilized to study HVC's electrophysiology, more specifically, *in vitro* electrophysiology using patch clamping technique. Experiments were implemented in accordance to the National Science Foundation guidelines and approved by the University of Chicago Animal Care and Use Committee. Intracellular patch clamping required the sacrifice of the zebra finches while maintaining the health of their HVC neurons. Artificially replicating the environment of the songbird's brain throughout the data collection process was essential in order to mimic the electrophysiological activity in the HVC neurons of a healthy and living zebra finch. To do so, artificial cerebrospinal fluid (ACSF) was prepared using a preexisting recipe [19], and brain slicing was followed to allow access to HVC projecting neurons that are found at 1200 micrometers in the cerebrum when cut at sagittal planes. Once HVC projecting neurons were accessed and located, patch clamping was proceeded to collect electrophysiological activity from HVC projecting neurons.

3.1.1 ACSF Preparation

To maintain the health of the songbird's brain, two different ACSF solutions were prepared. One was glucose based, and the other was sucrose based. The glucose based ACSF contained NaCl (119mM), KCl (2.5mM), $MgCl_2$ (1.3mM), $CaCl_2$ (2.5mM), NaH_2PO_4 (1.0mM), $NaHCO_3$ (26.2mM), Glucose (22mM) (osmolarity 285–295 mosM), and KOH solution was added for adjusting pH of ACSF to 7.2pH-7.3pH. Glucose based ACSF was used to maintain brain slices while patch clamping, it is sodium based since sodium is known to be a neuron-exciting compound. The sucrose based ACSF contained sucrose (72mM), NaCl (83mM), $MgCl_2$ (3.3mM), $CaCl_2$ (0.5mM), NaH_2 PO_4 (1.0mM) 26.2 $NaHCO_3$ (26.2mM), and glucose (22mM, osmolarity 285–295mosM) and pH was adjusted to 7.2pH-7.3pH by adding KCl. Sucrose based ACSF was used to maintain the health of the whole brain while brain slicing to stop any excitability.

3.1.2 Intracellular Solution Preparation

Intracellular recordings require breaking the cellular membrane of a neuron and recording the voltage difference between the inside of the neuron with respect to the outside medium (ACSF). To do so without disrupting the intracellular medium or introducing variables into the membrane that could interfere with the normal activity of the neurons, intracellular solution was prepared to mimic the intracellular medium of the neuron. This solution was made of mM quantities of K-gluconate (100mM), $MgCl_2$ (5mM), EGTA (10mM), Na_2-ATP (2mM), Na_3-GTP (0.3mM), and HEPES (40mM), and the solution pH was adjusted to 7.2pH–7.3pH with KOH. The prepared intracellular solution was placed in

a -80°C freezer and later thawed and transferred to electrodes before the patching procedure.

3.1.3 Electrode preparation

To record intracellularly from neurons without damaging their cell membrane characteristics; micrometer electrode tips were prepared. The electrodes were pulled using a Sutter Instruments (Novota, CA) P-80 device to an average of 4-9 M Ω resistances. Patch clamping requires one electrode per neuron approach, so many electrodes were pulled in the process. Electrodes had to be changed with each approached neuron due to the fact that the intracellular solution in the electrode gets mixed with the one in the neuron when the neuron is approached, disturbing the next neuron's synaptic activity measurements. Also, leftover cell membrane from the approached neuron could be stuck on to the electrode tip, affecting the electrode's resistance and as a result affecting the patch clamp procedure when approaching a new neuron.

3.1.4 Brain Slicing

Once solutions and electrodes were prepared, the experiment commenced. First, the bird was collected from the breeding colony, and then it was anesthetized with isoflurane. Once its heartbeat slowed down to about 1 Hz, the bird was rapidly decapitated and the brain was surgically removed and placed in iced sucrose ACSF. The cerebellum was cut out and removed (not used in this research), then the cerebrum was cut midsagittaly to access the HVC on each hemisphere, all was done inside the iced sucrose ACSF to slow down neuron excitability and consequently neural death. HVC was identified as a slightly

whiter region on the forebrain. Both hemispheres were glued to a vibrating microtome stage in a position that allowed cutting sagittal slices of HVC. In the vibrotome (8A), the hemispheres were covered in sucrose ACSF with O_2 and CO_2 gases fed into solution to prolong the brain's health while being sliced. Once HVC was reached, 200-micrometer slices were prepared (2 slices per hemisphere, thereby dissecting all of HVC's volume). Slices were placed in 37 degree centigrade pre-warmed glucose ACSF solution chamber (Figure 8B) to mimic the brain temperature in a living songbird, with O_2 and CO_2 gases continuously fed into solution. The slices were incubated for 15 minutes before patching is commenced to allow the slices to recover and regain normal activity.

A **B**

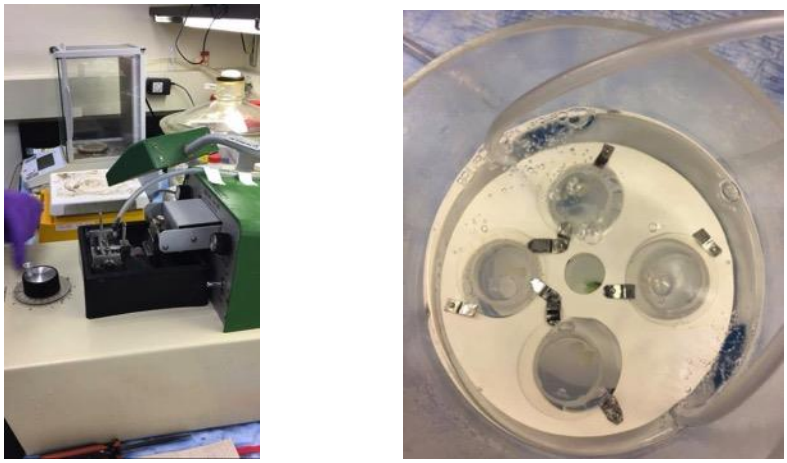

Figure 8: **A** Two-cerebral hemispheres being sliced using a vibrotome. **B** Sagittal brain slices being incubated and gassed with O_2 in a brain slice keeper prior to recording.

3.1.5 Patch Clamping

Incubated slices were moved to the light microscope (Figure 9A) and were drowned into continuously gassed glucose-based ACSF to keep the neuron nourished and healthy, since patching takes time, sometimes around 7 hours to patch through all healthy neurons in one slice. Before whole-cell patching was commenced, the slice was inspected using the light microscope, trans-illumination to locate HVC, which is a dark region in the slice due to its dense myelination (Figure 3). Once HVC was located, an electrode was filled with intracellular fluid, and the rest of the intracellular fluid was kept on ice to slow down ATP breakdown. Once a healthy neuron was localized, it was approached with the electrode until the electrode tip touched the neuron's cell membrane, increasing the electrode's resistance. Negative pressure was then applied to the electrode to create a gigaohm seal between the electrode and the cell membrane making the electrode tip a part of the cell membrane, and allowing for accurate measurements of electrophysiological activity of the neurons.

Each neuron was filled with biocytin (Figure 5) and was depolarized with a series of current steps of 200 or 400ms with 10pA to 200pA and 20 or 30pA steps, and hyperpolarized with a series of current steps of 200 or 400ms with -10pA to -120pA and 20pA or 30pA steps [19]. Cells that showed a stable resting membrane potential of below -55mV were recorded for further analysis (Figure 9B). HVC projecting neurons were identified according to electrophysiological characteristics as mentioned in Chapter 1 section 1.2.2. Electrophysiological recordings were completed using Multiclamp 700B (Axon Instruments, Foster City, CA), with an active bridge circuit for passing current, and

digitized (Digidata 1322A; Axon Instruments), all whilst connected to a computer running Axon pClamp 9 acquisition software (Molecular Devices, Sunnyvale, CA) [19] . Data was collected from two classes of HVC neurons; HVC_{RA} and HVC_{X} (Figure 10), but analysis in this study will be focused on HVC_{RA} neurons.

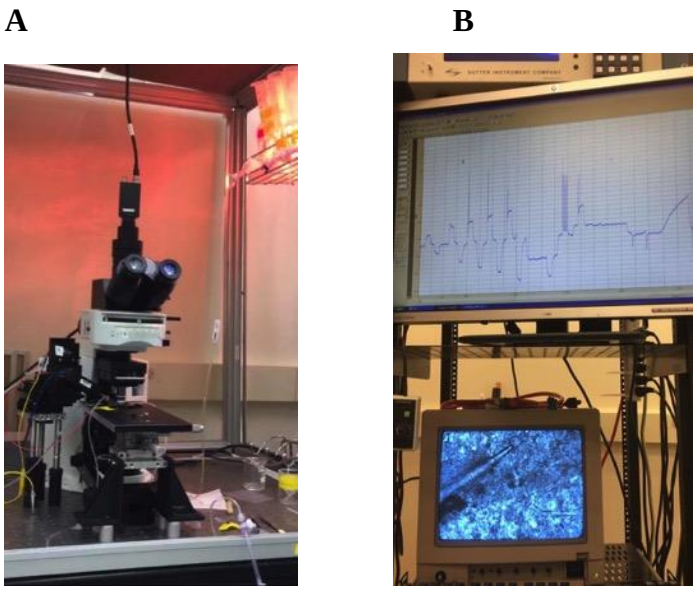

Figure 9: Patch clamping setup giving real time electrophysiological data. **A**. The rig where slices are held for recording. **B**. Neural recordings were collected via the help of specialized software where data was digitized and stored.

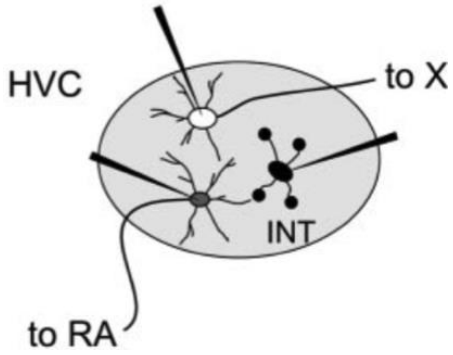

Figure 10: Schematic of electrophysiological collection of firing pattern in HVC projecting neurons; HVC_{X}, and HVC_{RA} [18].

3.2 Computational Modeling

Computational modeling was carried according to a single-compartment conductance-based biophysical model of HVC neurons completed in 2013 [19]. The model was simulated using MATLAB (MathWorks) and will be available online for other's usage. The functional forms of activation/inactivation gates and time constants were based on the published Daou et al. 2013 model [19]. Ionic channels were added and removed from the Daou et al. 2013 model to fit the HVC_{RA} firing patterns. Once ionic channels were chosen, the membrane potential of every HVC_{RA} neuron obeyed the updated model equation from Chapter 1 section 1.2.3. The model parameters (described next) were adjusted manually to reproduce firing patterns of HVC_{RA} similar to the data collected from HVC_{RA} neurons firing in response to applied step currents. Varying model parameters of each corresponding ionic channel allowed for fitting the spike upstroke and down-stroke, the amplitude interspike interval, the adaptation, and the sag of action potentials as elaborated in Chapter 1 section 1.2.2. The model fit was considered appropriate if the model voltage trace replicated the spike frequency, time, amplitude and resting membrane potential of the voltage trace collected electrophysiologically. The credibility of the model was established if the model provided good predictions when presented with data sets different than the ones used to fit it [19].

CHAPTER 4

RESULTS

4.1 Experimental Results

Electrophysiological data was collected (n=36 birds) in accordance to the methodology mentioned in Chapter 3 section 3.1. All data was simulated, filtered (butterworth notch filter) and plotted using MATLAB (MathWorks). Firing patterns were identified to be HVC_{RA} or HVC_X (Figures 11, 12) respectively, in line with the electrophysiological characteristics set by previous literature as mentioned in Chapter 1.

HVC_{RA} Biological Trace

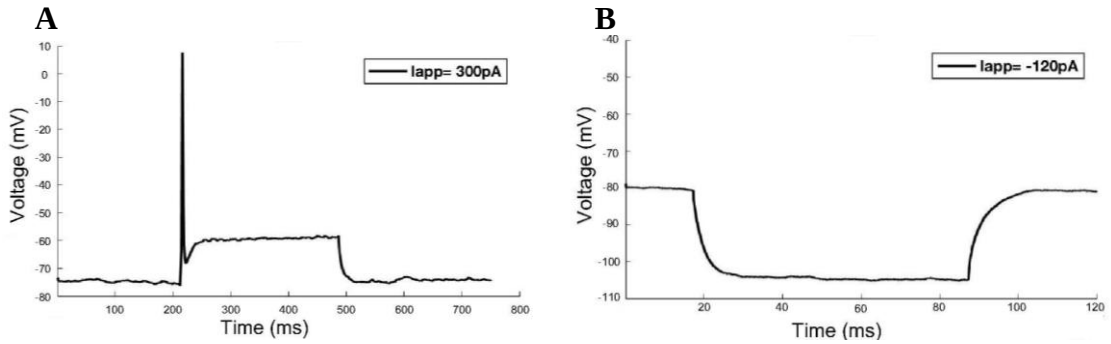

Figure 11: A sample HVC_{RA} neuron response to depolarizing (**A**, 300 pA) and hyperpolarizing (**B**, -120 pA) current pulses.

HVC_X Biological Trace

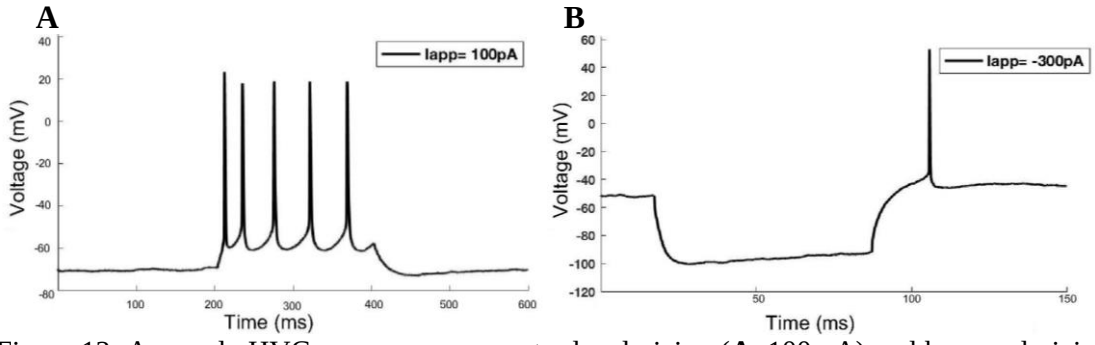

Figure 12: A sample HVC_X neuron response to depolarizing (**A**, 100 pA) and hyperpolarizing (**B**, -300 pA) current pulses showing sag.

4.2 Modifications to the Daou et al. 2013 Model of HVC_{RA}

Hodgkin Huxley (H-H) was initially used as the backbone for this research's single compartment model of HVC_{RA} neurons, with only sodium (I_{Na}), potassium (I_K) and leak (I_L) currents. This basic spiking model conforms the following equation [22]:

$$C_M\frac{dV}{dt} = -I_{Na} - I_K - I_L + I_{app}$$

In order to fit this simple H-H model to the experimentally collected HVC_{RA} current-clamp electrophysiological data, currents were included in accordance to the Daou et al. 2013 model of HVC. As mentioned in Chapter 1 section 1.2.3, the Daou et al. 2013 model satisfied the following equation [19]:

$$C_M\frac{dV}{dt} = -I_{Na} - I_K - I_L - I_{Ca-T} - I_{Ca-L} - I_A - I_{SK} - I_{KNa} - I_h - I_{Nap} + I_{app}$$

However, as mentioned earlier, this model needs improvement as it exhibits a mean square error of 34.81 (Figure 13), so modifications were done to it accordingly.

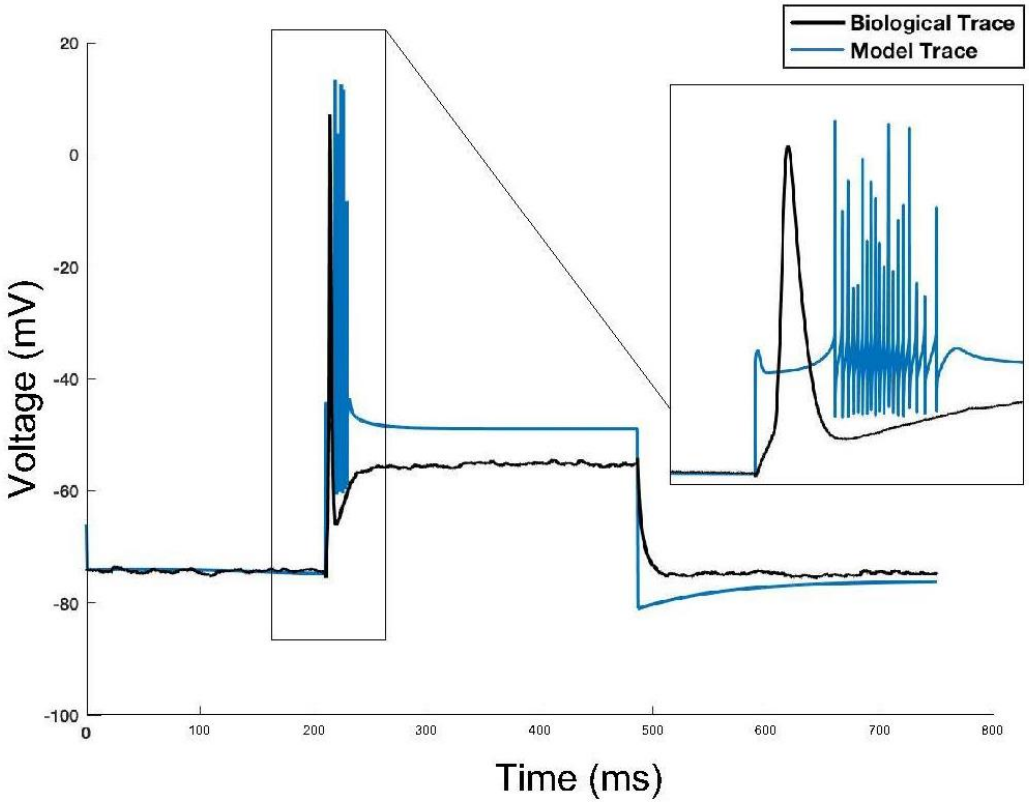

Figure 13: Daou et al. 2013 model of HVC_{RA} projecting neurons with mean error of 34.81.

4.2.1 Currents Maintained

In short, the first three currents in the Daou et al 2013 model (I_{Na}, I_K, I_L) satisfy the H-H model mentioned above, as they are part of every neuron in the brain, and so they were maintained in this model. Another important current also retained was the high threshold calcium current, $I_{Ca\text{-}L}$ responsible for burst firing in HVC neurons, since this current was proven to exist by Long et al. in 2010 [28]. Also, HVC_{RA} neurons usually elicit one to two action potentials in the form of bursts when given a considerably large positive depolarizing current pulse, making $I_{Ca\text{-}L}$ applicable in this model. Another current salvaged from the 2013 model is the calcium dependent potassium current, I_{SK}, which is primarily

responsible for adaptation in HVC neurons and was assumed to have the same effect in HVC_{RA} neurons due to their strong adaptation. The hyperpolarization cation current, or I_h shows no effect due to depolarizing current pulse; however it is responsible for the sag present in HVC_X and HVC_{INT} neurons. This feature is absent in the electrophysiological firing pattern response to hyperpolarizing pulses in HVC_{RA}, and has also not been proven to exist biologically, which prompted the removal of I_h from this model. However, when testing the updated model on negative current pulses (hyperpolarizing currents), I_h was inevitable. As such, slow and fast components of I_h were maintained from the 2013 model in a manner that weighs out the slow component in I_h, which is responsible for the sag (and which will be described next). Although a few of the currents in the Daou et al. 2013 model were conserved, some were also removed to accommodate the firing pattern of HVC_{RA} projecting neurons in response to depolarizing and hyperpolarizing current pulses.

4.2.2 Currents Removed

Some of the currents mentioned in the Daou et al. 2013 model are responsible for features that are absent in the electrophysiological firing pattern of HVC_{RA}. One of those currents is the low threshold calcium current, or $I_{Ca\text{-}T}$, which is responsible for the rebound firing in HVC neurons due to hyperpolarizing pulses [19]. This feature is absent in HVC_{RA}'s firing pattern, and has not been determined to exist biologically in HVC_{RA} neurons when Daou et al. 2013 attempted blocking it with Mibafradil, so $I_{Ca\text{-}T}$ was removed. Potassium dependent sodium current, or I_{KNa} was also removed, as it was not possible to test the presence of this current biologically due to the ambiguity of the current blockage from using quinidine as a nonselective blocker of I_{KNa} [19]. Another current that

was not included in this model is the sodium persistent current, or $I_{Nap,}$ which is responsible for the plateau potential in response to depolarizing current. In HVC_{RA} neurons, action potentials are fired once *in vitro* or in a burst manner *in vivo*, making I_{Nap} also theoretically irrelevant when modeling HVC_{RA}. The A-type potassium current, I_A is known to cause a delay to spike in HVC neurons, so it was also removed in this model, as the studied class of HVC_{RA} neurons (Class 2) in this research does not show any delay to spike (Daou et al. showed that there are two classes of HVC_{RA} neurons, under review). The removal of all these currents from the previous model was not enough to mimic HVC_R's firing pattern due to depolarizing and hyperpolarizing currents, and so new currents were added.

4.2.3 Currents Added

HVC_{RA} neurons show very strong adaptation when depolarized, which encouraged the idea that more than one adaptation current was present in this projecting neuron. One adaptation current found in literature was the M-type potassium current, where M reflects the current's response to pharmacological stimulation of Muscarinic (M) acetylcholine receptors [29]. The M-type current has both fast and slow components, I_{Ms} and I_{Mf} respectively [29]. Both components were implemented in the model since HVC_{RA} shows fast adaptation after its first and only action potential and slow persistent adaptation throughout further current injection. In theory this current was applicable, and this model's results show that it is in fact strongly responsible for HVC_{RA}'s unique strong adaptation.

4.3 New HVC_{RA} Model

With the above background, the finalized model designed for the membrane potential of each HVC_{RA} neuron includes spike-producing currents; I_K and I_{Na}, a leak current I_L, a high-threshold L-type Ca^{2+}current $I_{Ca\text{-}L}$, a Ca^{2+}-activated K^+ current I_{SK}, fast and slow M-type K^+ currents and a hyperpolarizing current I_h.

The membrane potential of each HVC_{RA} neuron obeys the below equation, and is conveyed through a circuit representation adapted from the H-H model (Figure 14):

$$C_m\frac{dV}{dt} = -I_K - I_{Na} - I_L - I_{Ca-L} - I_{SK} - I_{Ms} - I_{Mf} - I_h + I_{app}$$

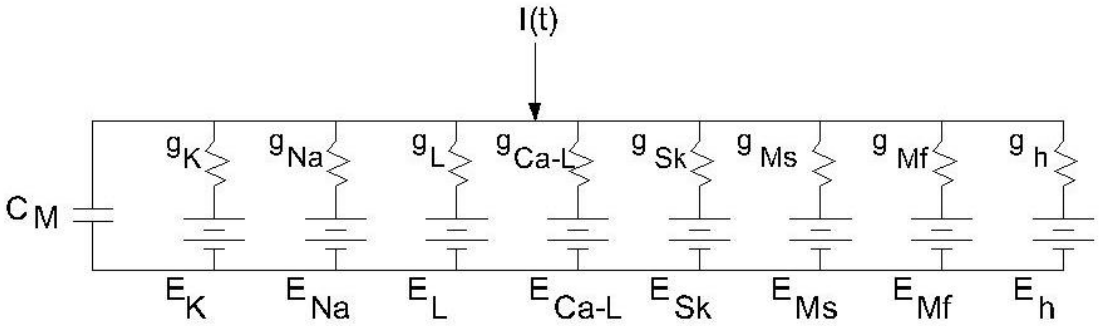

Figure 14: Circuit representation of the updated HVC_{RA} model highlighting the principal ionic currents integrated.

The voltage gated ionic currents obey the following equations (Figure 15) [19]:

$$I_K = g_K n^4 (V - V_K)$$

$$I_{Na} = g_{Na} m_\infty{}^4(V) h (V - V_{Na})$$

$$I_L = g_L (V - V_L)$$

$$I_{Ms} = g_{Ms} p (V - V_K)$$

$$I_{Mf} = g_{Mf} q (V - V_K)$$

$$I_h = g_h [k_r r_f + (1 - k_r) r_s (V - V_h)$$

$$I_{Ca-L} = g_{Ca} Vs_\infty{}^2(V) \left(\frac{Ca_{ex}}{1 - e^{\frac{2Fv}{RT}}} \right)$$

Where V(t) is the membrane potential, C_M is the membrane capacitance, I_{app} is the constant applied current. The maximal conductance for sodium, potassium, leak and hyperpolarizing currents respectively are: g_{Na}, g_K, g_L, g_h. The reversal potentials for sodium, potassium, leak and hyperpolarizing currents are: V_{Na}, V_K, V_L, V_h respectively. k_r is a parameter that directs the weight put on the fast component relative to the slow component (that characterizes the sag in response to a hyperpolarizing pulse) of the I_h current (Table 2), and as such k_r was given a large value in order to give almost all of the weight to the fast component of the I_h current and very little to the slow component.

The remaining current is the calcium dependent potassium current, which has an intracellular calcium concentration ($[Ca^{2+}]_i$) dependent gate, and as such follows the below equation (Figure 15) [19]:

$$I_{SK} = g_{SK} k_{\infty}([Ca^{2+}]_i)(V - V_K)$$

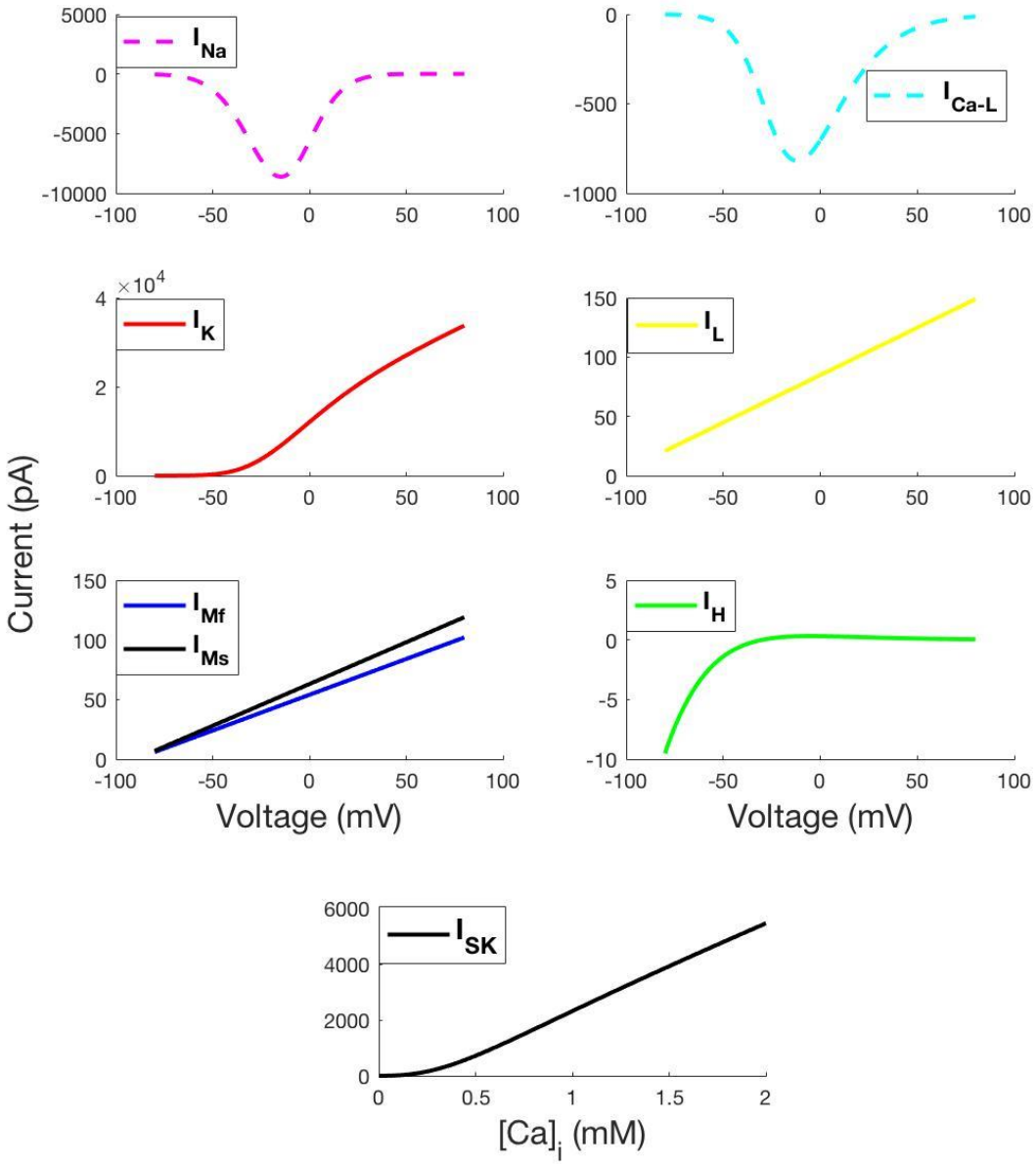

Figure 15: The voltage-dependent ionic currents are plotted as a function of voltage at equilibrium. Dashed lines represent inward currents, and solid lines represent outward currents. Bottom panel shows the Ca^{++}-dependent K^{+} current dynamics as a function of intracellular calcium concentration. The magnitude of each current indicates the currents' influence on the total behavior of the neuron.

4.3.1 Differential Equations

I_{Na} is the only current controlled by both activating and inactivating gating variables, m and h respectively. I_K, I_{Mf}, I_{Ms} and $I_{Ca\text{-}L}$ are activated by n, p, q and s gating variables respectively. The functional forms of the activation/inactivation gates are characterized as instantaneous, fast or slow by the equations below:

Fast gating variables treated as instantaneous, governed as follows (Figure 16 solid line):

$$x_\infty(\mathrm{V}) = \frac{1}{1 + \mathrm{e}^{(\frac{\mathrm{V} - \theta_x}{\sigma_x})}}$$

Where *x* is m_∞ and s_∞ for I_{Na} and $I_{Ca\text{-}L}$ respectively. θ_x is the half-activation voltage for gating variable *x* and σ_x is the slope factor (Table 2).

Slow gating variables governed by first order kinetics as follows (Figure 16 dashed line):

$$\frac{\mathrm{d}x}{\mathrm{dt}} = \frac{x_\infty(\mathrm{V}) - x}{\tau_x}$$

$$x_\infty(\mathrm{V}) = \frac{1}{1 + \mathrm{e}^{\frac{\mathrm{V} - \theta_x}{\sigma_x}}}$$

Where *x* is h and n for I_{Na} and I_K respectively. τ_x is the time for gate activation (Table 2).

Each current presented unique aspects of their differential equations:

I_{Na}:

$$h_\infty = \frac{\alpha_h}{\alpha_h + \beta_h}$$

$$\beta_H = \frac{4}{1 + e^{\frac{-(V+\theta_{bh})}{\sigma_{bh}}}}$$

$$\alpha_h = 0.128e^{\frac{-(V+\theta_h)}{\sigma_h}}$$

I_K:

$$\tau_n(V) = \frac{\overline{\tau_n}}{\cosh\frac{V - \theta_n}{2\sigma_n}}$$

I_{Ms}:

$$\frac{dp}{dt} = \alpha_P(1 - p) - \beta_P p$$

$$\beta_P = \frac{0.0001(V + \theta_P)}{-1 + e^{(\frac{V+\theta_P}{\sigma_P})}}$$

$$\alpha_P = \frac{-0.0001(V + \theta_P)}{-1 + e^{\frac{-(V+\theta_P)}{3}}}$$

$$p_\infty = \frac{\alpha_p}{\alpha_p + \beta_p}$$

I_{Mf}:

$$\frac{dq}{dt} = \alpha_q(1 - q) - \beta_q q$$

$$\alpha_q = \frac{-0.002(V + \theta_p)}{-1 + e^{\frac{-(V+\theta_p)}{\sigma_p}}}$$

$$\beta_q = \frac{0.002(V + \theta_p)}{-1 + e^{(\frac{V+\theta_p}{\sigma_p})}} + \frac{0.2(V + \theta_q)}{-1 + e^{(\frac{V+\theta_q}{\sigma_q})}}$$

$$q_\infty = \frac{\alpha_q}{\alpha_q + \beta_q}$$

I_h:

Fast activation component:

$$\frac{dr_f}{dt} = \frac{r_{f\infty}(V) - r_f}{\tau_{r_f}(V)}$$

$$r_{f\infty}(V) = \frac{1}{1 + e^{(\frac{V-\theta_{r_f}}{\sigma_{r_f}})}}$$

$$\tau_{r_f}(V) = \frac{p_{r_f}}{\frac{-7.4(V+70)}{e^{(\frac{V+70}{-0.8})} - 1} + 65e^{(\frac{V+56}{-23})}}$$

$$p_{r_f} = 100$$

Fast activation component:

$$\frac{dr_s}{dt} = \frac{r_{s\infty}(V) - r_s}{\tau_{r_s}}$$

$$r_{s\infty}(V) = \frac{1}{1 + e^{-(\frac{V-\theta_{r_s}}{\sigma_{r_s}})}}$$

τ_{r_s} = Constant (Table 2)

Steady state gating variable (Figure 16):

I_{SK}:

$$k_{\infty}([Ca^{2+}]_i) = \frac{[Ca^{2+}]_i^{\,2}}{[Ca^{2+}]_i^{\,2} + k_s^{\,2}}$$

$$k_s = 0.6\mu M$$

$$\frac{d[Ca^{2+}]_i}{dt} = -f(\varepsilon I_{Ca} + k_{[Ca^{2+}]_i}([Ca^{2+}]_i - 0.1))$$

$$f = 0.1$$

$$\varepsilon = 0.0015 pA^{-1} \cdot \mu M \cdot ms^{-1}$$

$$k_{[Ca^{2+}]_i} = 0.03 ms^{-1}$$

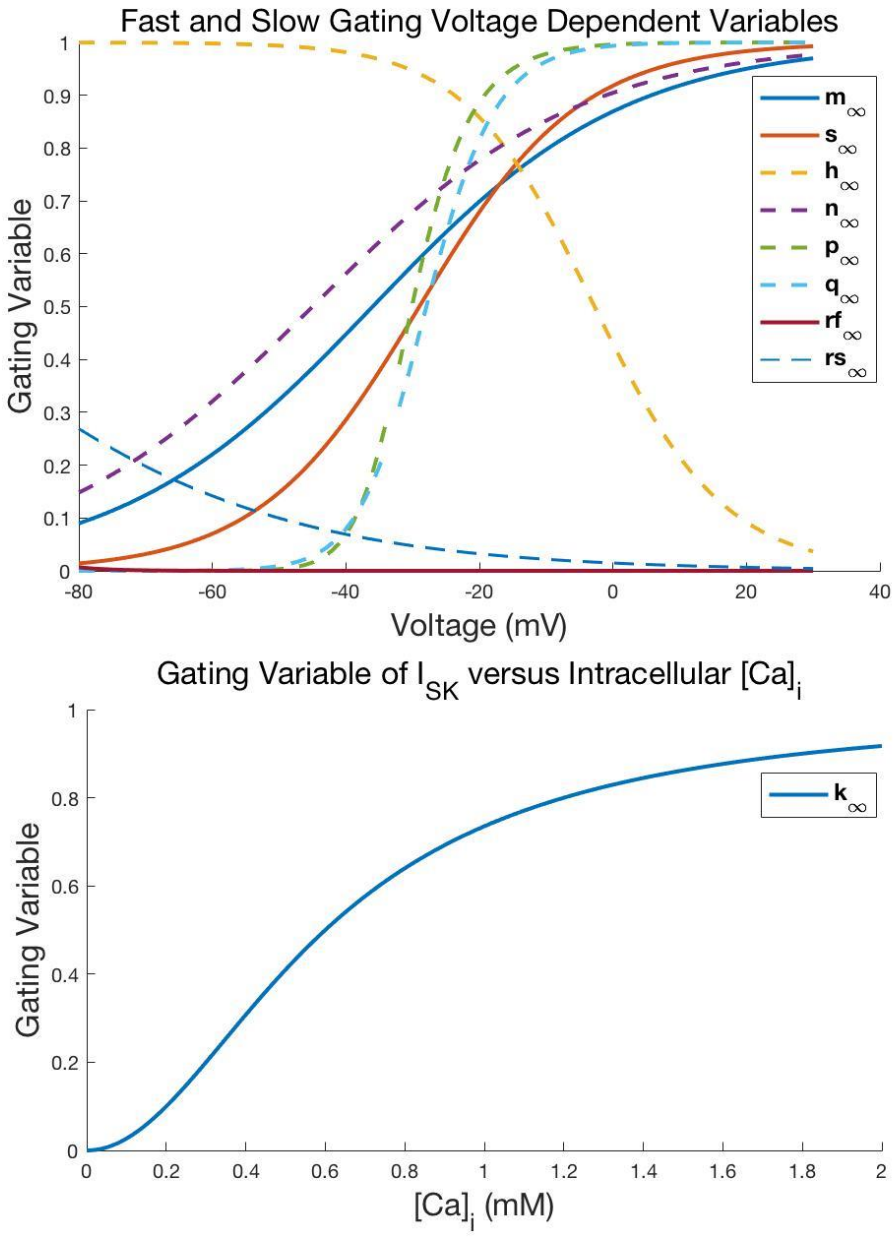

Figure 16: Voltage dependent gating variables, where dashed lines represent slow gating variables and solid lines represent fast or instantaneous gating variables of ionic channels. Calcium dependent potassium current is presented separately. These set of curves were used to help fit the model. For example steepness of the line and shiftiness in voltage direction dictate the rate of activation/inactivation and half-activation voltage of gating variables respectively.

Table 2: Parameter values used in model.

Parameter	Value	Parameter	Value
g_{Na}	400 nS	θ_{rf}	-105 mV
g_{K}	200 nS	θ_{rs}	-105 mV
g_{L}	0.8 nS	σ_{p}	6 mV
$g_{Ca\text{-}L}$	20 nS	σ_{h}	11 mV
g_{SK}	35 nS	σ_{bh}	35 mV
g_{Ms}	70nS	σ_{m}	-19 mV
g_{Mf}	60 nS	σ_{n}	-20 mV
g_{h}	1 nS	σ_{h}	11 mV
θ_{bh}	15 mV	σ_{s}	-15 mV
θ_{h}	1 mV	σ_{rf}	5 mV
θ_{m}	-36 mV	σ_{rs}	25 mV
θ_{n}	-45 mV	τ_{rs}	1500 ms
θ_{s}	-29 mV	$\overline{\tau}_{n}$	10 ms
θ_{q}	68 mV	τ_{h}	0.9 ms
θ_{p}	33 mV	k_{r}	0.95

4.3.2 Model Fit

The goal behind this research was to identify the currents and parameters responsible for the firing pattern of HVC_{RA} projecting neurons in order to develop a biophysical model of HVC_{RA}. To do so, the parameters were manually fit to the electrophysiological data embodying current-clamp *in vitro* whole-cell recordings. The parameter values are described in Table 2. Ca_{ex} is 2.5mM signifies the external Ca^{2+} concentration, and RT/F is the term representing thermal voltage, where R is the gas constant, T is 25°C denoting temperature of bathing solution, and F is Faraday's constant. Reversal potential values V_{Na}, V_K, V_L and V_h are 50mV, -90mV, -106mV and -30mV respectively. $I_{Ca\text{-}L}$ and I_{SK} are potassium currents so they have the same reversal potential of potassium, which is equal to -90mV.

With the set of ionic currents described above and their associated parameters listed in Table 2, the model was able to replicate the firing pattern of HVC_{RA} neurons decently (Figure 17). In particular, both model and experimental HVC_{RA} traces exhibited strong adaptation where neurons fired once at the onset of current pulse; spike amplitude and spike width were comparable (mean square error of 3.97) as well as their resting membrane potentials. It was difficult with the old model to replicate any of these features, largely due to the wrong cocktail of ionic currents integrated. That being said, this model does not replicate the exact action potential features seen experimentally (Figure 17, inset), but that is not unexpected since there is no known mathematical model that can replicate all features of biological neurons.

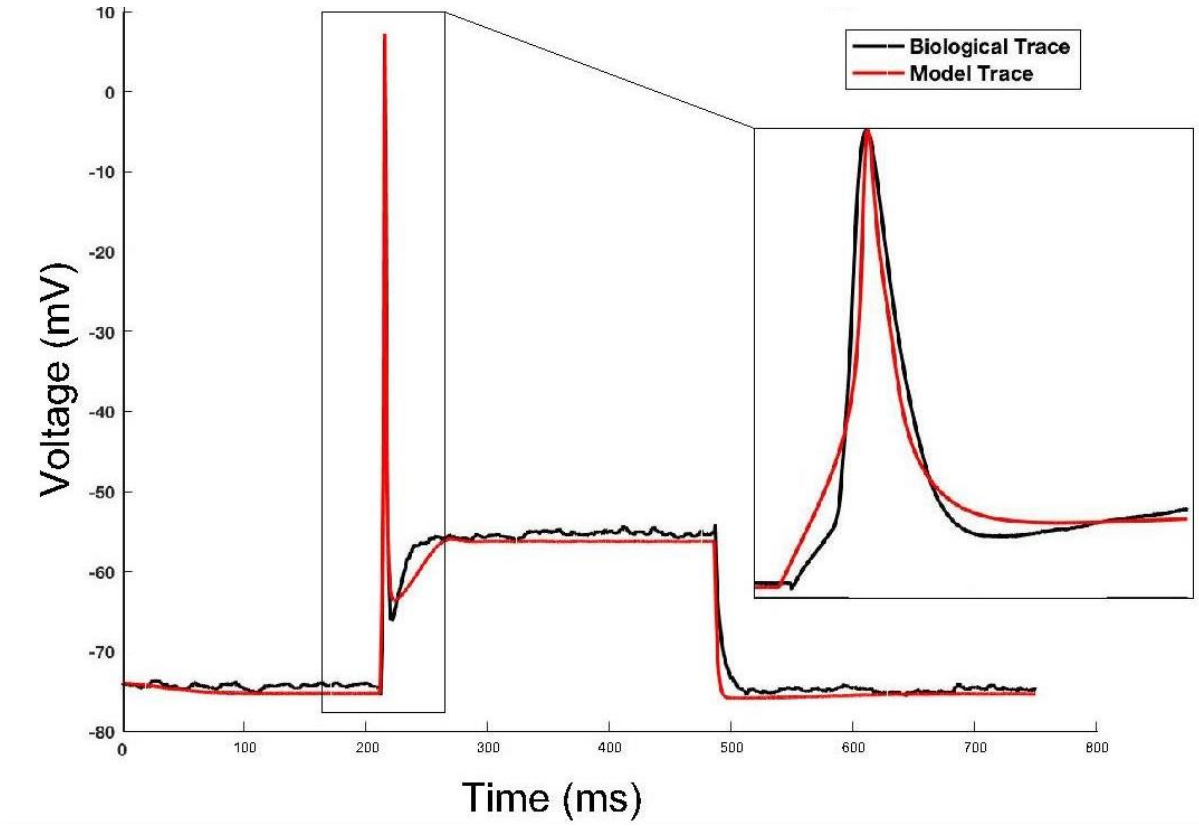

Figure 17: Model trace (red) overlaid with collected biological trace (black) when both were stimulated with 300 pA current pulse. The model generates a more or less decent fit to the biological trace. For the least, the spike amplitude and the spike width are matched, as well as the adaptation where both biological and model traces fire only once at the onset of current application.

4.4 Model Parameters in Relation to Model Fit

The effects of the model parameters on the features of HVC_{RA}'s firing pattern due to depolarizing current are shown through a heat map (Figure 18). Some features of the firing pattern were extracted quantitatively such as excitability, amplitude and spike width (Table 3, Figure 19, Figure 20). Other features could not be extracted quantitatively, so qualitative approximates were used, those include; after hyperpolarization (AHP), plateau, resting membrane potential (RMP beginning), resting membrane potential at the end of the firing pattern (RMP end). To represent the quantitative values in a heat map on a scale of -1 to 1, an error value was extracted according to the following sample calculations:

$$\text{Error} = \frac{\text{Feature value due to increased parameter} - \text{Feature value of biological trace}}{\text{Feature value of biological trace}}$$

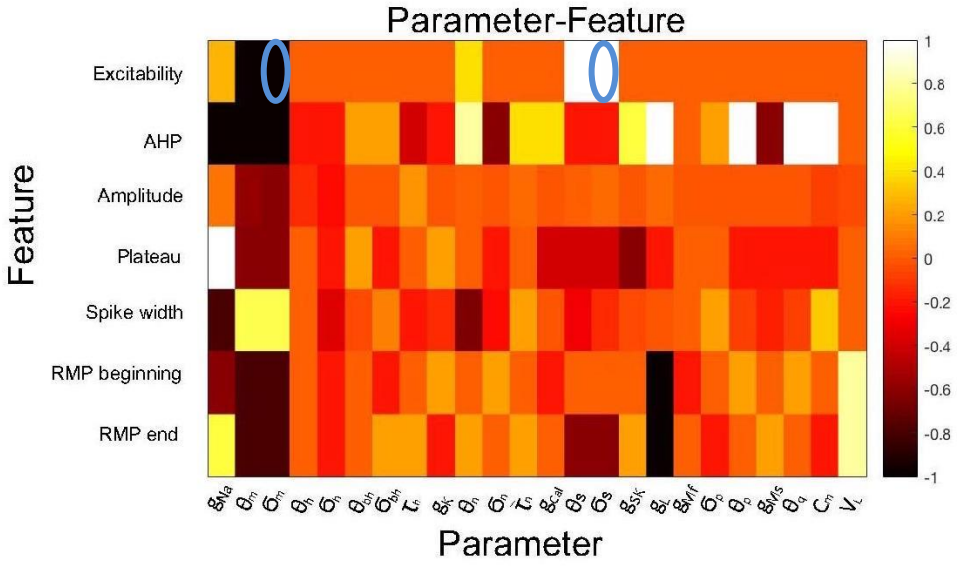

Figure 18: Heat map representing the effect of parameters on features of firing pattern. Feature represents firing pattern morphology, and parameter represents parameters used in differential equation. The strong presence of a feature due to parameter is expressed as 1 and strong absence of feature due to a parameter is represented as -1. Blue circles indicate the discussed parameter-feature relations in figures 18 and 19 below.

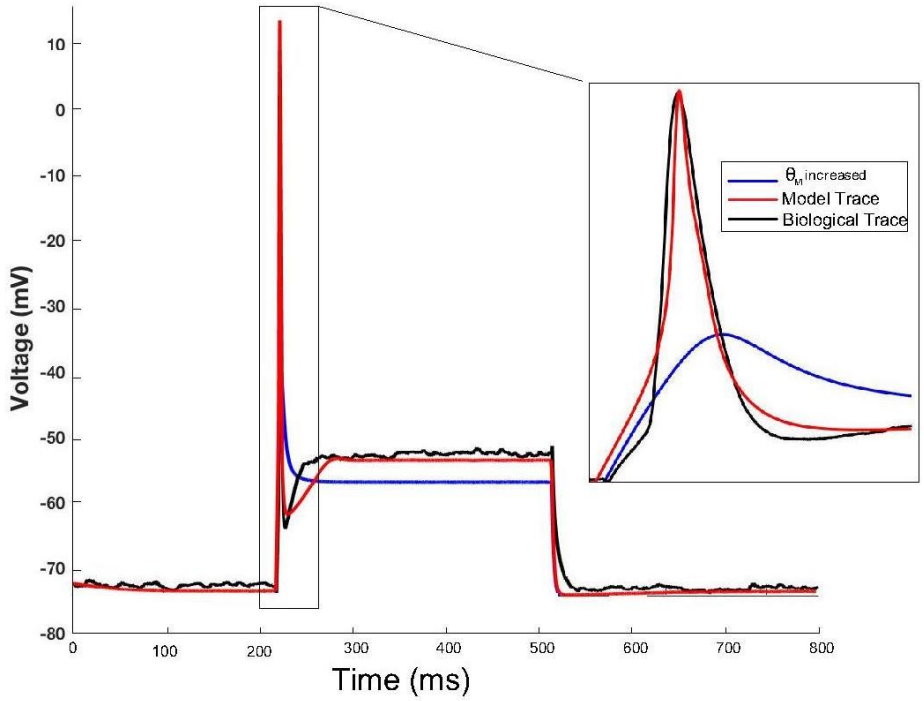

Figure 19: Plot with inset representing the strong effect of increasing θ_M on model fit excitability, justifying the appropriation of -1 to the heat map since excitability diminished.

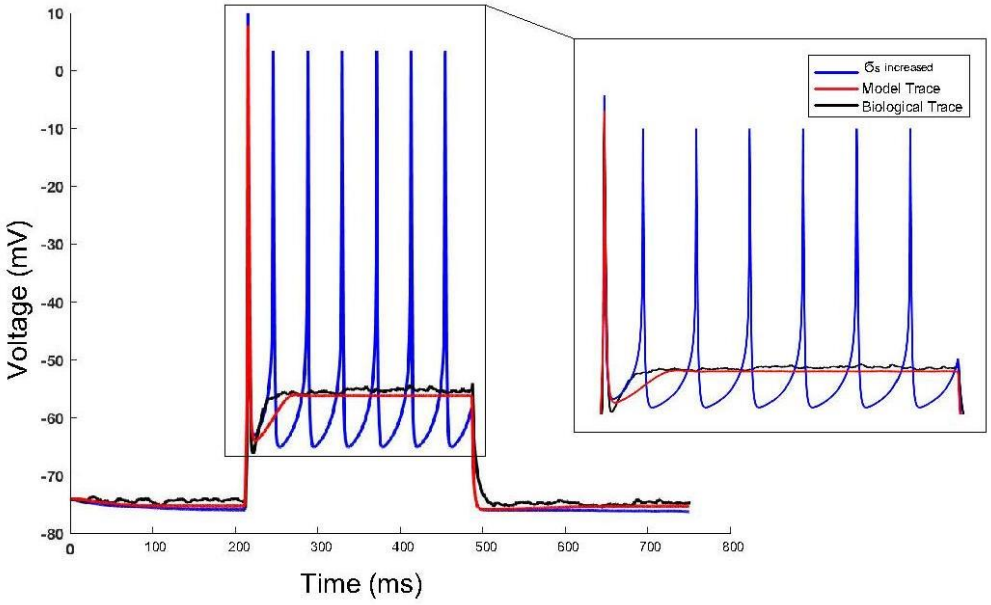

Figure 20: Plot with inset representing the effect of increasing σ_s on the model fit, justifying the appropriation of +1 to the heat map since excitability increased dramatically.

Table 3: This table shows a quantitative representation for some of the features expressed in the heat map. All parameter values were increased by a factor of 10 to quantify a uniform change amongst parameters. These values were translated onto the heat map through a -1 to 1 scale were -1 and +1 represent strong decrease or increase of feature respectively.

Feature / Parameter	Amplitude (mV)	Excitability (# of spikes)	Spike width
g_{Na}	81.2	3	0.006
θ_m	31.5	0	0.052
σ_m	30.3	0	0.052
θ_h	66	1	0.032
σ_h	57.5	1	0.02
θ_{bH}	74.1	1	0.03
σ_{bH}	76.7	1	0.035
τ_h	87.8	1	0.025
g_K	74.4	1	0.027
θ_n	78.2	4	0.011
σ_n	74.7	1	0.024
$\overline{\tau}_n$	78.4	1	0.038
$g_{Ca\text{-}L}$	75.8	1	0.031
θ_S	77.8	9	0.022
σ_S	80.6	7	0.027
g_{SK}	75.1	1	0.030
g_L	79.7	1	0.031
g_{Mf}	75.6	1	0.032

σ_P	75.7	1	0.038
θ_p	74.5	1	0.029
g_{Ms}	75.1	1	0.026
θ_q	74.5	1	0.029
C	70.6	1	0.042
V_L	73.5	1	0.032
Biological Trace	75.91	1	0.032

4.4.1 M-type Currents and Model Fit

It is important to mention that the great adaptation observed in HVC_{RA} is primarily due to the M-type currents and the SK current. The effect of the M-type currents on the model trace was represented separately in this research due to its novelty in modeling HVC_{RA} neurons (Figure 21). To understand the role of each M-type current, the fast M-type current (I_{Mf}) and the slow M-type current (I_{Ms}) were strongly represented separately in the new model by increasing their conductance. Figure 21 shows a strong effect of I_{Mf} on after-hyperpolarization and a decline in the action potential amplitude, I_{Ms} shows a weaker effect on after-hyperpolarization and a similar decline in the action potential amplitude. This makes sense biologically due to the fact that the slow M-type current is activated and deactivated slowly, making its effect weaker on the after-hyperpolarization portion and stronger on adaptation due to continuous depolarizing current.

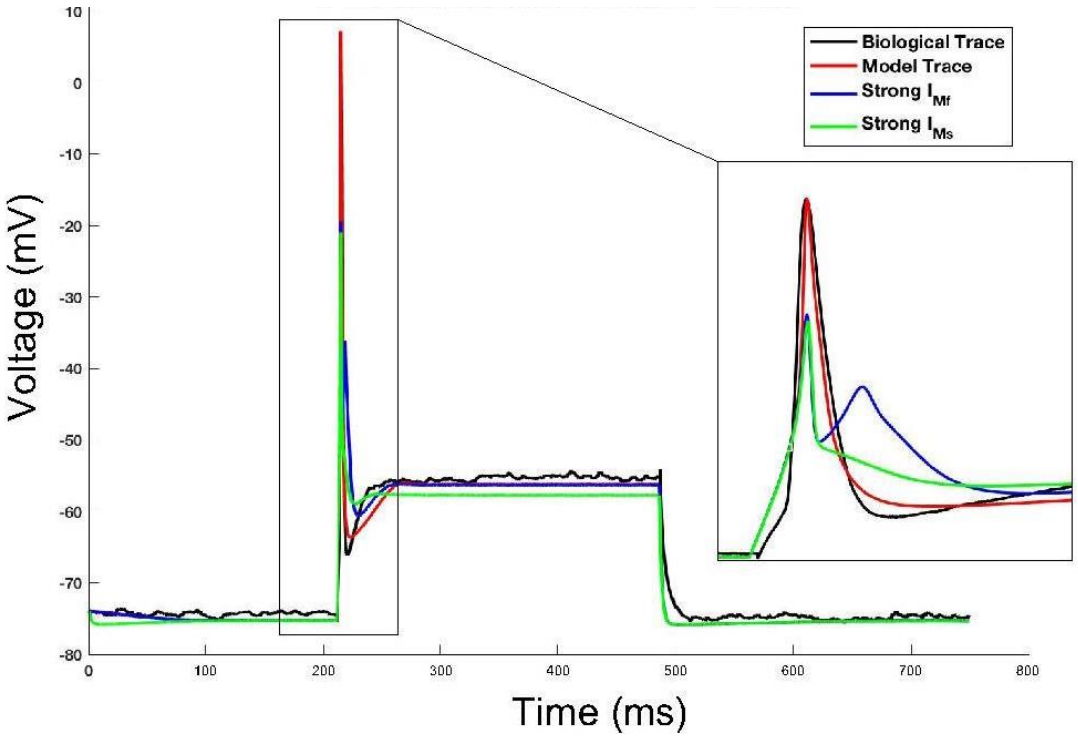

Figure 21: M-type currents fast (blue), slow (green) with their strength signified in terms of high conductance values, overlaid with the new model (red) and biological trace (black) to signify their separate effect in HVC_{RA} adaptation.

4.5 Model Testing

The modified parameters along with the removed and added currents from the Daou et al. 2013 model resulted in a model fit (Figure 17) with an improved mean square error of 3.97 in comparison to the older model (Figure 13) with a mean square error of 34.81. To further prove the model's accuracy, the model was tested on neurons that were not used to fit the model (Figure 22), and an average mean square error of 6.8 (Table 4) was shown indicating relatively good model accuracy. This better fit was obtained primarily due to the addition of the M-type K^+ currents, and it is important to mention that this current was never used in previous HVC_{RA} models. It is also significant to mention that as this is a

conductance based model, conductance values were changed within a certain biological range (Figure 23) to fit neurons of the two classes of HVC_{RA}. Moreover, neurons receive electrical stimulus in a chaotic fashion *in vivo*, and so to ascertain the model's accuracy, the model was fit to whole-cell recordings collected due to chaotic depolarizing and hyperpolarizing pulses. The model showed very strong fits when due to chaotic stimuli (Figure 24) indicating the model's accuracy in replicating HVC_{RA} electrophysiological firing pattern *in vivo*.

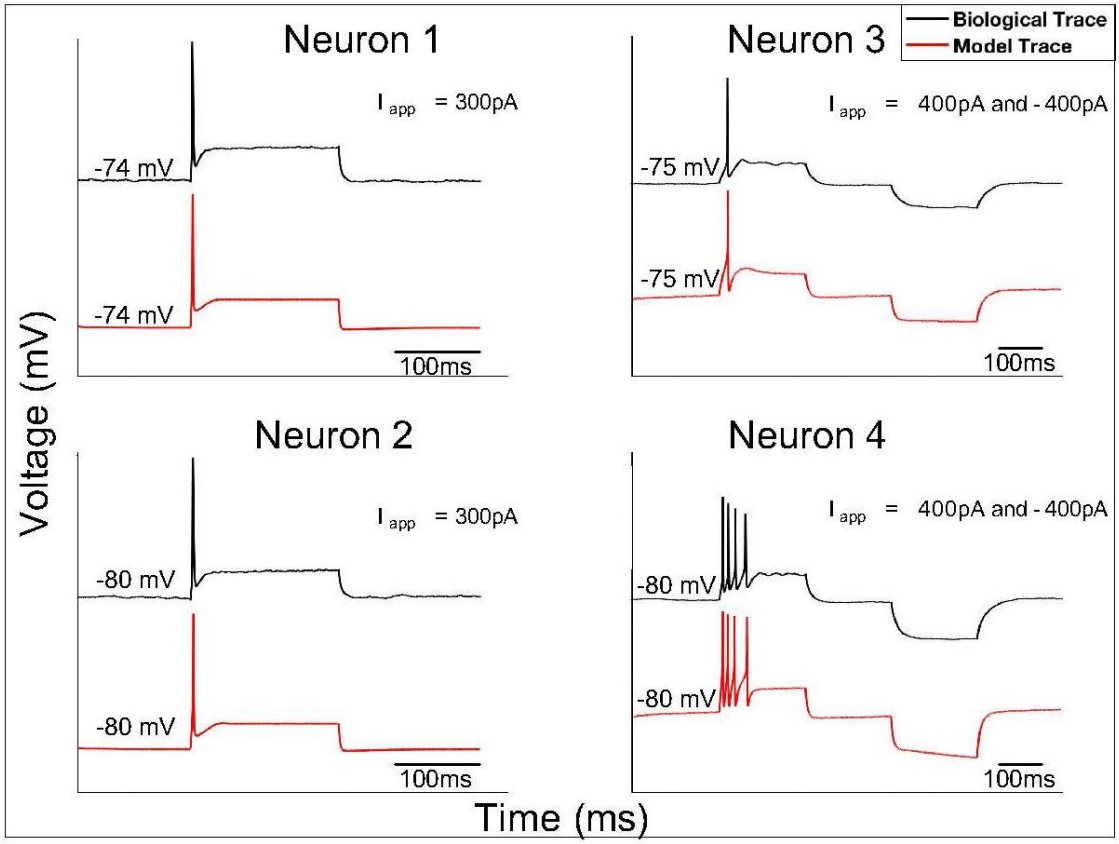

Figure 22: Panel showing model fit to four different neurons. Model fit (red) biological trace (black). Model fit shows close approximation of biological trace with similar resting membrane potential values (RMP) between model and biological trace, similar number of spikes, spike amplitude, and hyperpolarization response to hyperpolarizing current.

Table 4: Mean Square Error representation of test neurons.

Test Neurons	Mean Square Error
Neuron 1	5.7
Neuron 2	5.8
Neuron 3	7.7
Neuron 4	7.9
Average	6.8

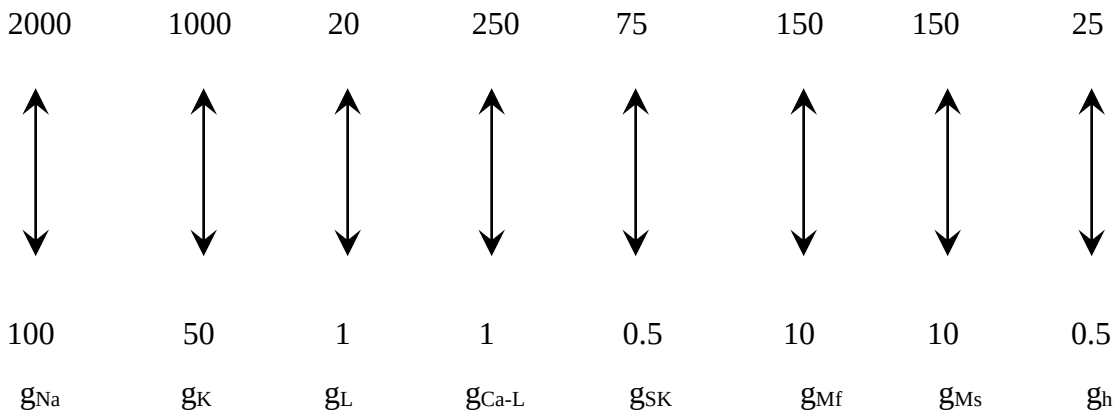

Figure 23: Conductance values were changed within a certain biological range when fitting the model to test neurons

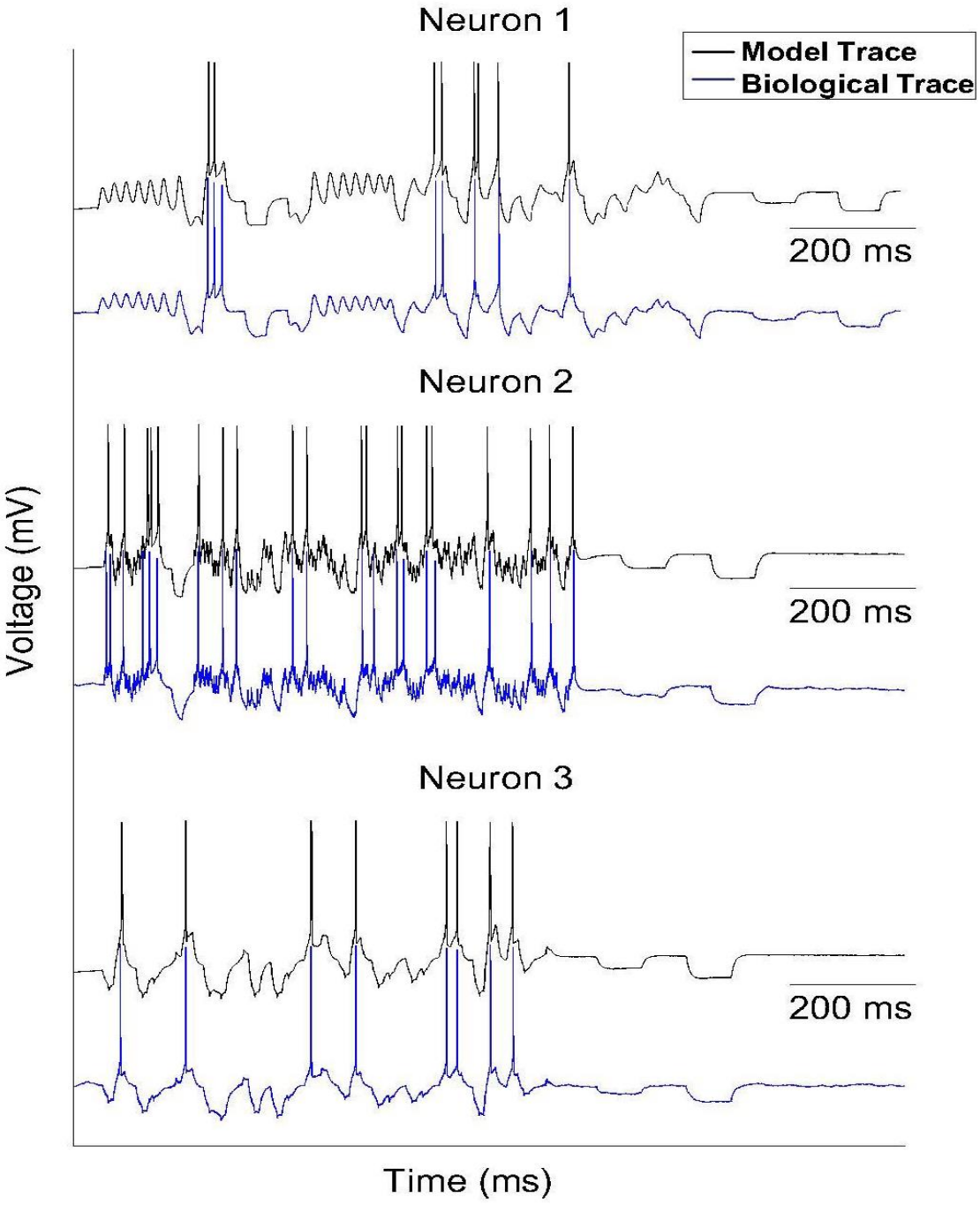

Figure 24: Panel showing model fit to three different neurons depolarized with chaotic current, to replicate *in vivo* electrical stimulus received by HVC_{RA} neurons. The model shows very good fits to chaotic stimulus indicating the model's accuracy in replicating HVC_{RA} electrophysiological firing pattern.

4.6 Geometric Analysis

According to this model, most of the currents acting on the HVC_{RA} neuron are voltage gated and as such, the total current acting on HVC_{RA} due to depolarizing current is affected as a function of voltage (Figure 25). The different stages of the membrane potential activate different currents, and this activation results in this new improved fit. According to such graphical representation, qualitative analysis in the form of geometrical analysis shows that this model is monostable [30], that is due to the fact that F(V) = dV/dt, so at every value of V where F(V) is negative, dV/dt is negative and so V decreases, and vice versa for positive values of F(V). This shows that the direction of movement of V and the progression of the dynamical system is determined by the sign of F(V) [30]. When dV/dt is 0, V is in equilibrium, and the membrane voltage is not changing. This model has three equilibria points, two of which are unstable, but only one stable point making it a monostable system (Figure 25). The total current is represented as regions of the sum of different currents, since currents are controlled by the relevant ionic channel gates, and the gates are activated as a function of voltage, the currents acting on these regions can be deduced from the voltage dependent gating variables (Figure 16), and as such for voltage between -80 mV and -30 mV, the sodium activating gate m_∞ is present and so I_{Na} is affecting the shape of the total current for this voltage region, and it is also shown that I_K inactivation gate is working in this region and so I_K is not present. $I_{Ca\text{-}L}$ is acting in this region due to the biological evidence of the calcium outward current influencing depolarization. The region between -30 mV and 0 mV is where I_{Na} and I_K and I_{Ca} are

acting, I_K begins activating to hyperpolarize the neuron, bringing back the action potential amplitude to 0 mV, and I_{Na} is inactivating as h_∞ is now employed. Once membrane potential reaches 0 mV, I_K is now the only current acting causing the after hyperpolarization region of the action potential, once I_K is not affecting the action potential, I_L acts as the only current on the membrane potential causing a return to RMP once the current is turned off.

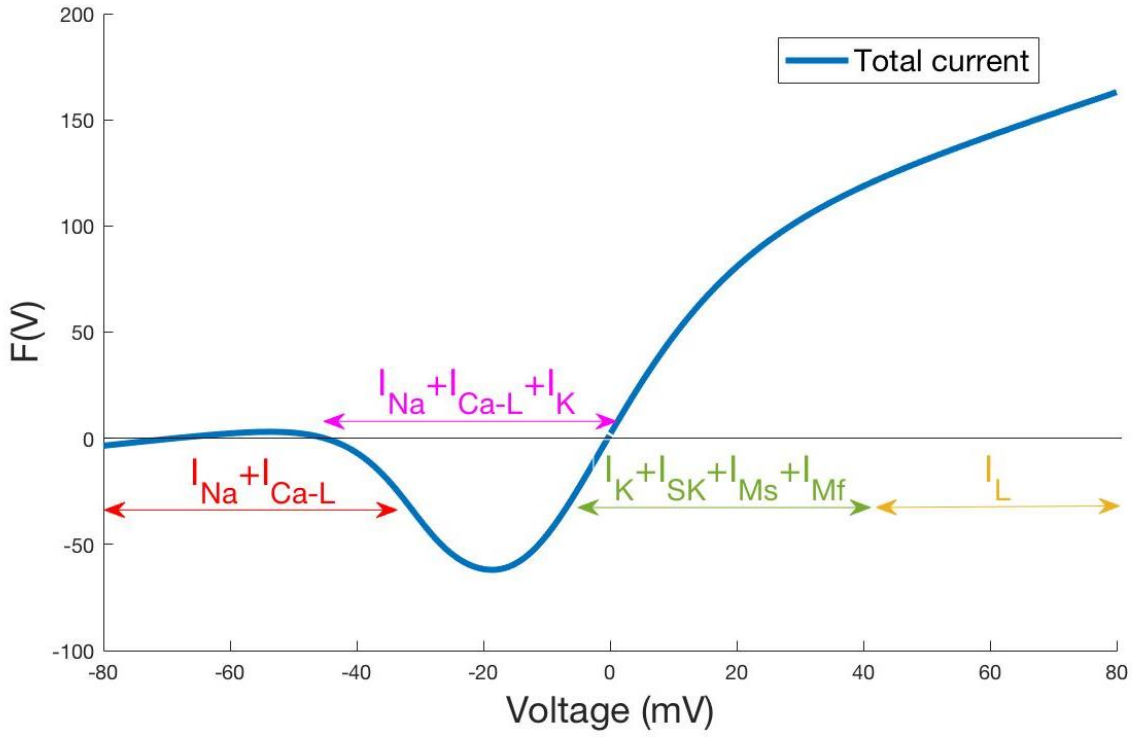

Figure 25: F(V) or dv/dt =-I_{Total}/C_m. Different currents affect the qualitative behavior of the model in accordance to the gating variables of each involved ionic channel. Stable equilibrium is represented as a black circle; unstable equilibra represented as hollow circles. The stability of the equilibria depicts the system monostable.

CHAPTER 5
DISCUSSION

HVC_{RA} projecting neurons are the motor neurons responsible for singing in HVC. Without HVC_{RA}, songbirds cannot articulate their songs due to the lack of motor stimulus. There is no existing model that properly replicates the electrophysiological firing pattern of HVC_{RA}, and so the neuroscience society lacks the information on the components of HVC_{RA} neurons, or in other words the currents acting on such neurons. Modeling HVC_{RA} will allow for a better understanding of the currents involved in the firing pattern of HVC_{RA}. This research presents an improved model of the electrophysiological firing pattern of HVC_{RA} zebra finch neurons through the identification of the currents or ionic channels present on neuron's cell membrane. The model was based on current-clamp recordings collected at the University of Chicago, which are consistent with the morphological and electrophysiological classifications of HVC_{RA} as mentioned in Chapter 1. Properties that include spike threshold, after hyperpolarization, amplitude and time to peek, were in accordance with the literature mentioned in Chapter 1.

Modeling these neurons allowed for the understanding of the role of the different ionic currents in molding the firing pattern of the HVC_{RA}. This model identifies seven currents, five of which are outward currents (I_K, I_L, I_{SK}, I_{Ms}, I_{Mf}), and two are inward currents (I_{Na} and $I_{Ca\text{-}L}$). A schematic summary of mentioned currents (Figure 26) depicts

that the variation in the balance (conductance value) of these various ionic currents shapes the firing properties of HVC_{RA} neurons. The schematic also includes a comparison with the Daou et al. 2013, model which shows that HVC_{RA} was modeled without the T-type calcium activated potassium current ($I_{Ca\text{-}T}$), the A-type potassium current (I_A), or the sodium activated potassium current (I_{KNa}).

Previous models have failed to replicate the firing pattern of HVC_{RA}, one notable model by Gibb et al in 2009 based on a single compartment H-H model, hypothesized that the sparse bursting in HVC_{RA} neurons was due to inhibitory interneurons terminating bursts in HVC_{RA} [29]. Their model is a network type model and in theory is possible, but further research carried by Daou et in 2013 rendered this model biologically inaccurate, by showing that HVC_{RA} fires intrinsically *in vitro*, and not due to any synaptic activity [29]. This means that the sparse bursting and high adaptation seen in HVC_{RA} is due to intrinsic properties and not due to HVC interneuron inhibitions [29]. Also, the Gibb model did not provide a biological trace to model trace comparison since intrinsic properties of HVC_{RA} were not studied [29]. Though the Gibb et al 2009 model was proven wrong by the Daou et al. model of 2013, the Daou et al. 2013 model is also not accurate in terms of modeling HVC_{RA} due to the difference in the spike properties between the model and the electrophysiological trace (Figure 13).

The new model shows important results as it indirectly proves the absence of (I_{KNa}, $I_{Ca\text{-}T}$, I_A, I_{Nap}) since even upon their removal, the firing pattern of HVC_{RA} was possible to replicate. Moreover, the addition of the M-type currents to the new HVC_{RA} model is

important, as it has been proven to reduce the firing of action potentials in mammalian neurons, and has a role in the control of neuronal excitability by limiting repetitive firing and maintaining the resting membrane potential [31] and as such is responsible for adaptation. M-type currents are also activated close to the resting membrane potentials, and as such counteract membrane depolarization and respond to muscarinic (M) acetylcholine receptor agonists, hence the name. Research has also shown that such currents (slow and fast) have to coexist for the adaptation to work properly [32]. Mutations in the M-type channels have shown to be associated to epilepsy, the benign familial neonatal convulsions, which are known to present clonic seizures, and as such are rhythmic [32]. This demonstrates a role of the M-type currents in rythmogenesis that is relevant in HVC_{RA} as song production is rhythmic in terms of signal propagation.

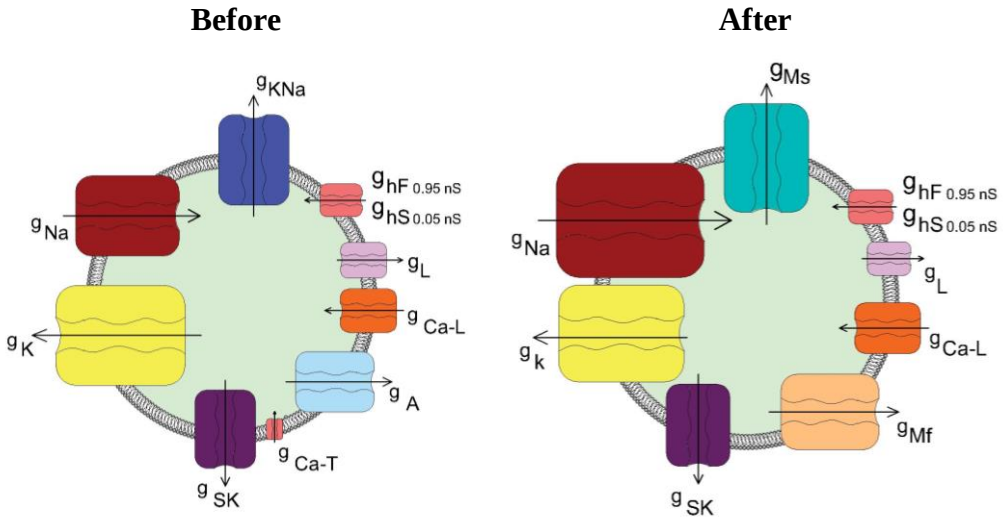

Figure 26: Schematic diagram portraying the ionic currents responsible for HVC_{RA} firing pattern from the previous (**Before**) model and new (**After**) model. The size of the ionic channels illustrates

the magnitude of the conductance parameters for the different currents involved (size computed based on logarithmic scale).

CHAPTER 6

CONCLUSION

The new HVC_{RA} model is imperative in developing an improved neural network that demonstrates the structure of the nucleus of the neurons in HVC. However, to further prove the accuracy of this model, pharmacological changes to the neurons should be conducted to ascertain the presence of mentioned currents. Pharmacological changes could be carried through the use of respective current blockers, and the analysis of the resulting electrophysiological pattern, if no change in biological trace, then current is definitely absent in the neuron. Blockers that could be used to prove this model are the linopirdine and its analogue XE991 for M-type K^+ channels respectively [33], TTX to block sodium channel for the Na^+ current, 4-Aminopyridine to block potassium channel for the K^+ channel, apamin to block the calcium dependent potassium channel for the SK current, and gabapentin to block the high threshold calcium channel for the high threshold calcium channel. The leak current is always available in cells so no need to test for its existence pharmacologically. Once pharmacological testing is finalized, a network adaptation of this model could be implemented.

This model is a single compartment model, an improvement could be done by creating a multicompartment model to represent the spatial aspect of the HVC neural

network, a model created by Armstrong et al in 2017 could be adapted to do so [34, 35]. The Armstrong model introduces a functional syllable unit (FSU) as a functional architect of HVC, and each FSU has two operations for inhibiting neurons, one is a simultaneous firing where inhibitory neurons fire synchronously and as such inhibitory neurons connect to excitatory neurons, another operation is competitive firing of the inhibitory neurons where patters of sequential firing of projection stabilized by the first operation could take place. The relation between different FSUs is responsible for song composition in HVC. This network could be adapted to the improved model by adding somatic and dendritic compartments as the "multicompartments" [34].

This model brings the songbird community a step closer to understanding the reason behind the change in spectral and temporal features of song, where sequential propagation of activity is disrupted after change in the firing pattern of HVC_{RA} neurons *in vivo* (Daou & Margoliash, under review). The model also provides for a healthy control to study the effect of one-ionic channel mutations in neurodegenerative diseases on vocalization.

BIBLIOGRAPHY

[1] C. Darwin, *The descent of man, and selection in relation to sex (book)*

Publisher vol. 2. Murray, London: D. Appleton, 1872.

[2] J. J. Bolhuis, K. Okanoya, and C. Scharff, "Twitter evolution: converging mechanisms in birdsong and human speech," *Nat Rev Neurosci,* vol. 11, pp. 747-59, Nov 2010.

[3] A. J. Doupe and P. K. Kuhl, "Birdsong and Human Speech - Common Themes and Mechanisms," 1999.

[4] E. H. Lenneberg, "The biological foundations of language." vol. 2, ed, 1967, pp. 59-67.

[5] M. M. Patterson and M. S. Fee, "Zebra Finches in Biomedical Research," pp. 1109-1134, 2015.

[6] R. H. Hahnloser, A. A. Kozhevnikov, and M. S. Fee, "An ultra-sparse code underlies the generation of neural sequences in a songbird," *Nature* 2002.

[7] D. Margoliash, "Functional Organization of Forebrain Pathways for Song Production and Perception," *Developmental Neurobiology* 1997.

[8] F. Johnson and M. Sellix, "Reorganization of a telencephalic motor region during sexual differentiation and vocal learning in zebra finches," *Elsevier* 2000.

[9] A. Reiner, D. J. Perkel, C. V. Mello, and E. D. Jarvis, "Songbirds and the Revised Avian Brain Nomenclature," *Annals New York Academy of Sciences,* 2004.

[10] H. Williams, "Birdsong and Singing Behavior," *Annals New York Academy of Sciences,* 2004.

[11] L. Kubikova, E. Bosikova, M. Cvikova, K. Lukacova, C. Scharff, and E. D. Jarvis, "Basal ganglia function, stuttering, sequencing, and repair in adult songbirds.," *Scientific reports,* 2014.

[12] S. C. Woolley and M. H. Kao, "Variability in action: contributions of a songbird cortical-basal ganglia circuit to vocal motor learning and control.," *Neuroscience,* 2015.

[13] R. Mooney, "Neural mechanisms for learned birdsong," *Learn Mem,* vol. 16, pp. 655-69, Nov 2009.

[14] D. Margoliash, "Sleep, Learning, and Birdsong," *ILAR,* 2010.

[15] J. M. Wild, M. F. Kubke, and R. Mooney, "Avian Nucleus Retroambigualis: Cell Types and Projections to Other Respiratory-Vocal Nuclei in the Brain of the Zebra Finch (Taeniopygia guttata)," *NCBI,* 2009.

[16] R. Mooney, W. Hoese, and S. Nowicki, "Auditory representation of the vocal repertoire in a songbird with multiple song types," *Proceedings of the National Academy of Sciences,* 2000.

[17] R. Mooney, "Different Subthreshold Mechanisms Underlie Song Selectivity in Identified HVc Neurons of the Zebra Finch," *The Journal of Neuroscience,* 2000.

[18] R. Mooney and J. F. Prather, "The HVC microcircuit: the synaptic basis for interactions between song motor and vocal plasticity pathways," *J Neurosci,* vol. 25, pp. 1952-64, Feb 23 2005.

[19] A. Daou, M. T. Ross, F. Johnson, R. L. Hyson, and R. Bertram, "Electrophysiological characterization and computational models of HVC neurons in the zebra finch," *J Neurophysiol,* vol. 110, pp. 1227-45, Sep 2013.

[20] M. Kubota and I. Taniguch, "Electrophysiological Characteristics of Classes of Neuron in the HVc of the Zebra Finch," *Journal of Neurophysiology,* 1998.

[21] P. Dutar, H. M. Vu, and D. J. Perkel, "Multiple Cell Types Distinguished by Physiological, Pharmacological, and Anatomic Properties in Nucleus HVc of the Adult Zebra Finch," *Journal of Neurophysiology,* 1998.

[22] A. L. Hodgkin and A. F. Huxley, "A quantitative description of membrane current and its application to conduction and excitation in nerve.," *The Journal of physiology,* 1952.

[23] M. Kubota and N. Saito, "Sodium and Calcium-Dependent Conductances Of Neurones In The Zebra Finch Hyperstriatum Ventrale Pars Caudale In Vitro," *Journal of physiology,* 1991.

[24] K. K. Jain, "Ion Channels and Neurological Disorders," *MedLink Neurology,* 1999.

[25] P. Kumar, D. Kumar, S. K. Jha, N. K. Jha, and R. K. Ambasta, "Ion Channels in Neurological Disorders," *Adv Protein Chem Struct Biol,* vol. 103, pp. 97-136, 2016.

[26] H. Lerche, K. Jurkat-Rott, and F. Lehmann-Horn, "Ion channels and epilepsy," *Am J Med Genet,* vol. 106, pp. 146-59, Summer 2001.

[27] P. Kumar, D. Kumar, S. J. Kumar, N. J. Kumar, and R. K. Ambasta, "Advances in Protein Chemistry and Structural Biology. Chapter Three - Ion Channels in Neurological Disorders," *Science Direct,* vol. 103, 2015.

[28] M. A. Long, D. Z. Jin, and M. S. Fee, "Support for a synaptic chain model of neuronal sequence generation," *Nature,* vol. 468, pp. 394-9, Nov 18 2010.

[29] L. Gibb, T. Q. Gentner, and H. D. Abarbanel, "Inhibition and recurrent excitation in a computational model of sparse bursting in song nucleus HVC," *J Neurophysiol,* vol. 102, pp. 1748-62, Sep 2009.

[30] E. M. Izhikevich, *Dynamical systems in neuroscience*: MIT press, 2007.

[31] I. Dorange and B.-M. Swahn, "Recent Progress in the Discovery of Kv7 Modulators," vol. 46, pp. 53-65, 2011.

[32] G. Avanzini, "Intrinsic Properties of Neocortical Neurons Relevant to Seizure Discharges: The Lesson of Epileptogenic Channelopathies," *Elsevier* 2009

[33] E. Santini and J. T. Porter, "M-type potassium channels modulate the intrinsic excitability of infralimbic neurons and regulate fear expression and extinction," *J Neurosci,* vol. 30, pp. 12379-86, Sep 15 2010.

[34] E. Armstrong and H. D. I. Abarbanel, "Model of the Songbird Nucleus HVC as a Network of Central Pattern Generators," 2017.

[35] B. J. Carroll, R. Bertram, and R. L. Hyson, "Intrinsic physiology of inhibitory neurons changes over auditory development," *Journal of Neurophysiology,* vol. 119, pp. 290-304, 2017.

[36] A. J. Doupe and M. Konishi, "Song-selective auditory circuits in the vocal control system of the zebra finch," *Neurobiology,* 1991.

[13, 14, 19, 36]